TECHNICAL REPORT BRL-TR-2788

THE INFLUENCE OF CONVERGENCE-VELOCITY GRADIENTS ON THE FORMATION OF SHAPED-CHARGE JETS

MILES L. LAMPSON

MARCH 1987

US ARMY BALLISTIC RESEARCH LABORATORY
ABERDEEN PROVING GROUND, MARYLAND

DISCLAIMER NOTICE

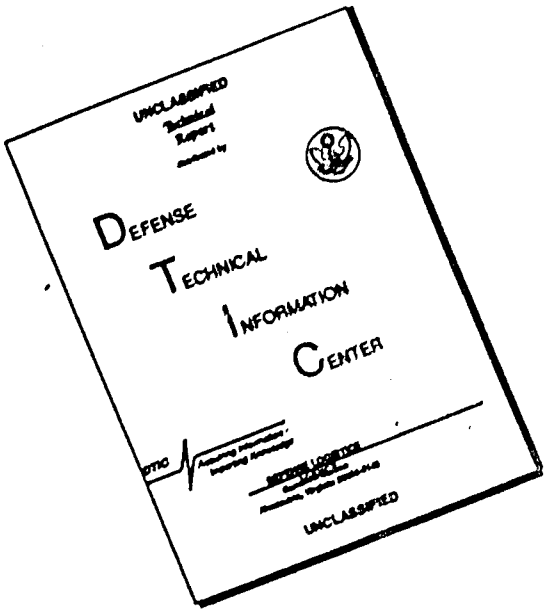

THIS DOCUMENT IS BEST QUALITY AVAILABLE. THE COPY FURNISHED TO DTIC CONTAINED A SIGNIFICANT NUMBER OF PAGES WHICH DO NOT REPRODUCE LEGIBLY.

Destroy this report when it is no longer needed.
Do not return it to the originator.

Additional copies of this report may be obtained from the National Technical Information Service, U. S. Department of Commerce, Springfield, Virginia 22161.

The findings in this report are not to be construed as an official Department of the Army position, unless so designated by other authorized documents.

The use of trade names or manufacturers' names in this report does not constitute indorsement of any commercial product.

UNCLASSIFIED

SECURITY CLASSIFICATION OF THIS PAGE

REPORT DOCUMENTATION PAGE

Form Approved
OMB No 0704-0188
Exp Date Jun 30 1986

1a REPORT SECURITY CLASSIFICATION: Unclassified	1b. RESTRICTIVE MARKINGS
2a SECURITY CLASSIFICATION AUTHORITY	3. DISTRIBUTION / AVAILABILITY OF REPORT
2b DECLASSIFICATION / DOWNGRADING SCHEDULE	
4 PERFORMING ORGANIZATION REPORT NUMBER(S)	5. MONITORING ORGANIZATION REPORT NUMBER(S)
6a. NAME OF PERFORMING ORGANIZATION: Ballistic Research Laboratory; 6b. OFFICE SYMBOL (If applicable): SLCBR-TB	7a. NAME OF MONITORING ORGANIZATION
6c. ADDRESS (City, State, and ZIP Code): Aberdeen Proving Ground, MD 21005-5066	7b. ADDRESS (City, State, and ZIP Code)
8a. NAME OF FUNDING / SPONSORING ORGANIZATION; 8b OFFICE SYMBOL (If applicable)	9 PROCUREMENT INSTRUMENT IDENTIFICATION NUMBER
8c. ADDRESS (City, State, and ZIP Code)	10. SOURCE OF FUNDING NUMBERS

PROGRAM ELEMENT NO	PROJECT NO	TASK NO	WORK UNIT ACCESSION NO
1L263636D223			

11 TITLE (Include Security Classification)

The Influence of Convergence-Velocity Gradients on the Formation of Shaped-Charge Jets

12 PERSONAL AUTHOR(S)
Lampson, Miles L.

13a TYPE OF REPORT	13b TIME COVERED	14 DATE OF REPORT (Year, Month, Day)	15 PAGE COUNT
TR	FROM _____ TO _____		

16 SUPPLEMENTARY NOTATION

17 COSATI CODES		
FIELD	GROUP	SUB-GROUP
20	14	

18. SUBJECT TERMS (Continue on reverse if necessary and identify by block number)
shaped-charge theory, convergence effects
jet formation theory, jet characteristics

19. ABSTRACT (Continue on reverse if necessary and identify by block number)

The radial collapse of an axisymmetric shell necessarily generates a velocity gradient through the thickness of the shell. The existence of this gradient is ignored in the previous analytical treatment of the jet formation from such shells. The effect of this "convergence-velocity" gradient on the partition of mass and velocity in jets from the explosively-driven collapse of conical, metallic shells is discussed.

20 DISTRIBUTION / AVAILABILITY OF ABSTRACT	21 ABSTRACT SECURITY CLASSIFICATION
☐ UNCLASSIFIED/UNLIMITED ☐ SAME AS RPT ☐ DTIC USERS	Unclassified

22a NAME OF RESPONSIBLE INDIVIDUAL	22b TELEPHONE (Include Area Code)	22c OFFICE SYMBOL
Miles L. Lampson	301/278-6069	SLCBR-TB-W

DD FORM 1473, 84 MAR — 83 APR edition may be used until exhausted; All other editions are obsolete

SECURITY CLASSIFICATION OF THIS PAGE
UNCLASSIFIED

TABLE OF CONTENTS

FIGURES

FIGURES CONTINUED

TABLES

I. INTRODUCTION

The importance of the shaped-charge warhead as an antitank weapon has justified repeated efforts to analyze the phenomena associated with its performance. The conventional shaped-charge munition consists of a cylindrical charge of high explosive with an axisymmetric, conical cavity at one end into which is inserted a conical, metallic shell. On detonation of the explosive from a point on the axis of symmetry of the charge at the end opposite the cavity, a pressure wave propagates toward the conical metal "liner," and passes over it, sequentially collapsing the shell and generating a high-velocity stream of metal, called the "jet" and a lower velocity, more massive body, called the "slug." The jet travels along the axis of symmetry of the system, in the direction of the propagation of the detonation wave, and is capable of penetrating the high-strength steel used to protect military vehicles.

Much of the research done on shaped-charge physics in England and in the United States during the Second World War was summarized in 1948 in an article by Garrett Birkhoff, Duncan MacDougall, Emerson Pugh and Sir Geoffrey Taylor.[1] These authors derived equations describing the jet generated by the symmetrical collapse of a hollow, ductile wedge under steady flow conditions. Because of the extremely-high pressures acting on the explosively-driven metal wedge, the wedge material was treated as a hydrodynamically-perfect fluid. Although not strictly applicable to the collapse of hollow cones, this theory was used to predict the mass and velocity of jets from conventional shaped-charge munitions and the predictions were in good agreement with the experimental data for the first-formed portions of these jets.

The steady-state theory of jet formation from wedge-lined charges was modified in 1952 by Emerson Pugh, Robert Eichelberger, and Norman Rostoker[2] to account for the variation in the collapse velocity imparted to the wall of the metal shell of a conventional shaped charge. The introduction of variable-flow input conditions into the steady jet-formation theory resulted in a description of the velocity gradient found between the tip and tail of a conventional shaped-charge jet.

Experimental evidence supporting the theory of Pugh, Eichelberger and Rostoker was presented in 1952 by Eichelberger and Pugh.[3] By recovering the jet and "slug" material from conventional shaped charges with conical, steel liners and by measuring the velocity of different portions of the jet, the authors were able to show that, within the experimental error, the jets produced from collapsing cones were well-described by the "unsteady" jet formation theory valid for collapsing wedges.

By 1954, Eichelberger[4] had refined his experimental technique sufficiently to detect small but systematic discrepancies between the observed characteristics of the jet from a collapsing cone and the characteristics predicted by the unsteady jet formation theory for collapsing wedges. He showed that the finite time required to accelerate the liner to its final collapse velocity, neglected in the usual theoretical treatment, did not explain the observed discrepancies. Another possible source of error in the theoretical treatment, neglect of the convergence-velocity gradient described by Sterne,[5] was suggested,[6] but not explored.

With the advent of the two-dimensional, Lagrangian, hydrodynamical computer codes, such as HEMP,[7] it became possible to compute in detail the initial motion of an axisymmetric, shaped-charge liner. Unfortunately, for most devices, the material distortion occurring in the jet formation region could not be successfully treated. However, these calculations emphasized the progressive thickening of the shell wall which occurs during the collapse of a conical shell. This "convergence effect" leads to a velocity gradient through the thickness of the shell which influences the jet formation process. Such convergence-velocity gradients were described by Sterne in 1950 and suggested as possible perturbing influences on the simple, hydrodynamic, jet-formation theory of Birkhoff, MacDougall, Pugh, and Taylor.[1]

In this report, the quantitative effect of the "convergence-velocity gradient" on the characteristics of the jets formed from collapsing cones is evaluated in the spirit of the previous analytical jet-formation models. A repartition of the mass and velocity in the jet, differing from the predictions of the classical theory, is shown to occur under these conditions.

II. THE CONVERGENCE-VELOCITY GRADIENT

Suppose that a fluid shell of mass m per unit length, with external radius r_2 and internal radius r_1, executes a purely radial contraction. If the fluid is incompressible and mass is conserved, it follows that

$$\frac{d}{dt} (r_2^2 - r_1^2) = 0 \tag{2.1}$$

and the quantity

$$r_0^2 \equiv r_2^2 - r_1^2 \tag{2.2}$$

is a constant of the motion. Equation (2.1) implies that

$$r_2 \dot{r}_2 = r_1 \dot{r}_1 \tag{2.3}$$

where $\dot{r}_1 \equiv \frac{dr_1}{dt}$. More generally, since the mass of the shell can be subdivided into smaller radial regions, Equation (2.1) implies

$$r\dot{r} = r_2\dot{r}_2 , \qquad r_1 < r < r_2 . \tag{2.4}$$

If $r_2/r_1 \approx 1$, there is initially a nearly linear velocity gradient through the thickness of the shell, with the highest velocity at the inner surface.

Sterne characterizes the shell motion by the variable x, the ratio of r_2 to r_o. Then, for example,

$$r_1 = r_o \sqrt{x^2 - 1} . \tag{2.5}$$

The kinetic energy per unit length of the cylinder is found by integrating the kinetic energy density per unit length over the radial extent of the cylinder. The incremental kinetic energy per unit length, dT, due to the element of mass dm, located between r and r + dr and having characteristic radial velocity $\dot{r}$, is

$$dT = \frac{1}{2}\dot{r}^2 \, dm. \tag{2.6}$$

Now

$$dm = 2\pi\rho r dr \tag{2.7}$$

where ρ is the mass density of the shell material, so

$$T = \int_{r_1}^{r_2} \rho\pi r\dot{r}^2 dr \tag{2.8}$$

Since $r\dot{r}$ is constant throughout the shell, it may be moved outside the integral and

$$T = \pi\rho \, r_2^2 \, \dot{r}_2^2 \int_{r_1}^{r_2} \frac{dr}{r} \tag{2.9}$$

$$= \frac{m}{2} \, r_o^2 \, x^2 \dot{x}^2 \ln \frac{x^2}{x^2 - 1} \tag{2.10}$$

This kinetic energy is assumed to remain constant, so the radial velocity of any lagrangian element of mass, μ, may be found from

$$\dot{r}_\mu = \frac{r_2 \dot{r}_2}{r_\mu} \tag{2.11}$$

where $\mu = \pi\rho\,(r_2^2 - r_\mu^2)$ (2.12)

Then

$$\dot{r}_\mu = \frac{r_2 \dot{r}_2}{\sqrt{r_2^2 - \mu/\pi\rho}} \tag{2.13}$$

$$= \frac{r_o x \dot{x}}{\sqrt{x^2 - \mu/m}} \tag{2.14}$$

But, from Equation (2.10),

$$x\dot{x} = \sqrt{\frac{2T}{m}}\ \frac{1}{r_o\sqrt{\ln\left[x^2/(x^2 - 1)\right]}} \tag{2.15}$$

so

$$\dot{r}_\mu = \frac{\partial r\,(\mu,t)}{\partial t} = \sqrt{\frac{2T}{m}}\ \frac{1}{\sqrt{\ln\left[x^2/(x^2 - 1)\right]}\ \sqrt{x^2 - \mu/m}} \tag{2.16}$$

The predictions of Sterne's theory for the radial collapse of a cylindrical shell which conserves its mechanical energy are shown in Figure 1. The copper shell has an initial external radius of 25mm, an initial external radial velocity of 1.5 km/s, and an initial internal radius of 23mm. The solid linesin Figure 1 represent the velocities of the inner, I, middle, M, and outer, O, parts of the shell. The dotted lines indicate the positions of these Lagrangian elements as the collapse parameter x changes. As the variable x approaches unity, the radial velocity of the internal surface approaches infinity and the velocity of all other elements of the shell approaches zero. Sterne points out that the rapid concentration of kinetic energy at the inner portion of the shell requires the generation of very large internal pressures.

Figure 2 shows the collapse-velocity vectors computed by the HEMP code for various Lagrangian elements of an explosively-driven conical shell which is collapsing toward its axis of symmetry. Only one-half of the cross-section of the conical segment is depicted. The values of the pressure field intensity (in GPa) at the centers of the HEMP computational cells are also given. The gradient of the velocity field through the thickness of the shell is apparent as well as the divergence of the shell boundaries as the flow approaches the axis. A wedge of equivalent initial thickness explosively-collapsed shows no such velocity gradient. The covergence-velocity gradient is then formed when the flow divergence velocities are superimposed on the explosively driven collapse velocity.

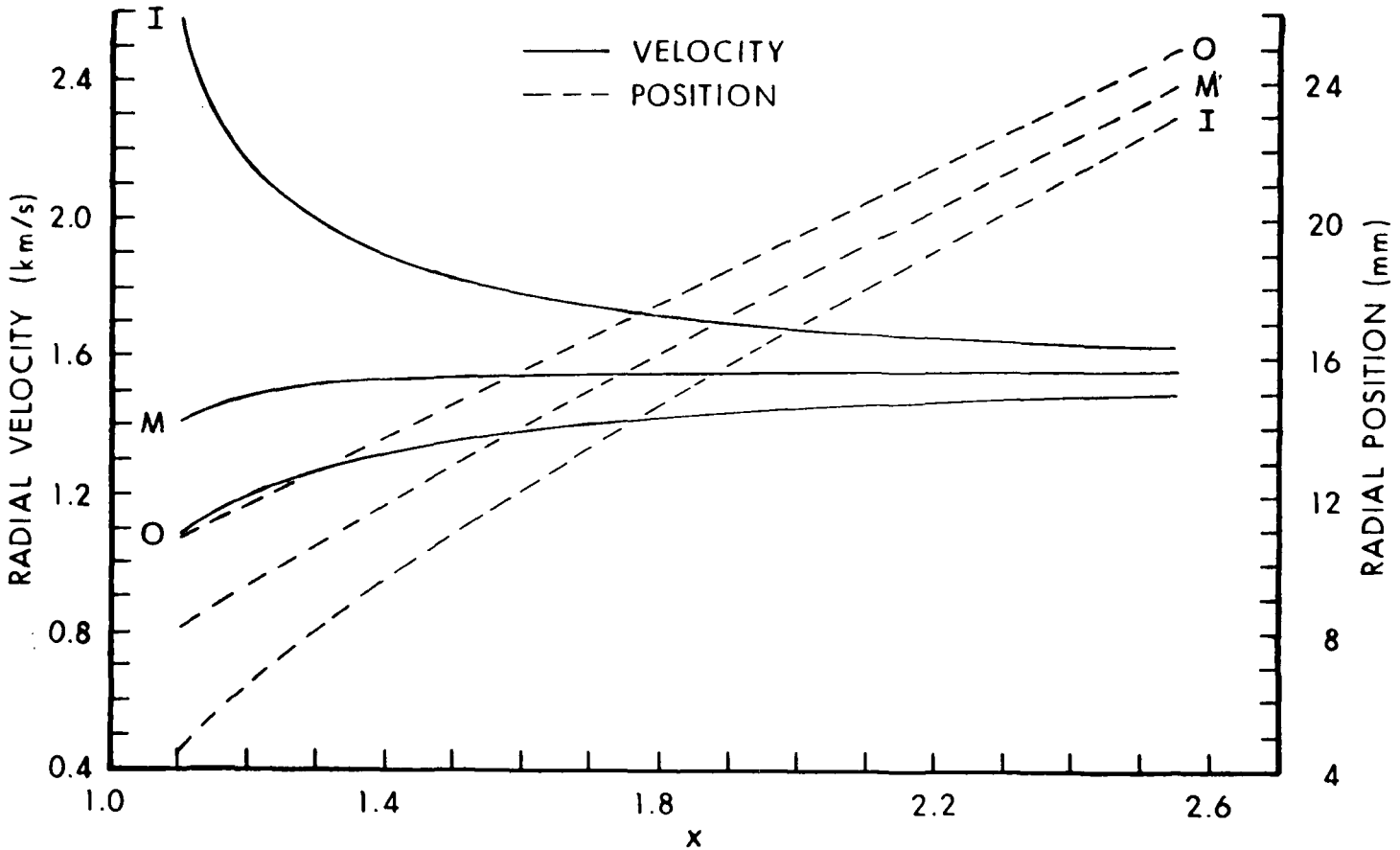

Figure 1. The development of flow divergence (dotted curves) and convergence velocity gradient (solid curves) in a radially collapsing cylindrical shell, as a function of the collapse parameter $x = r_2/r_o$.

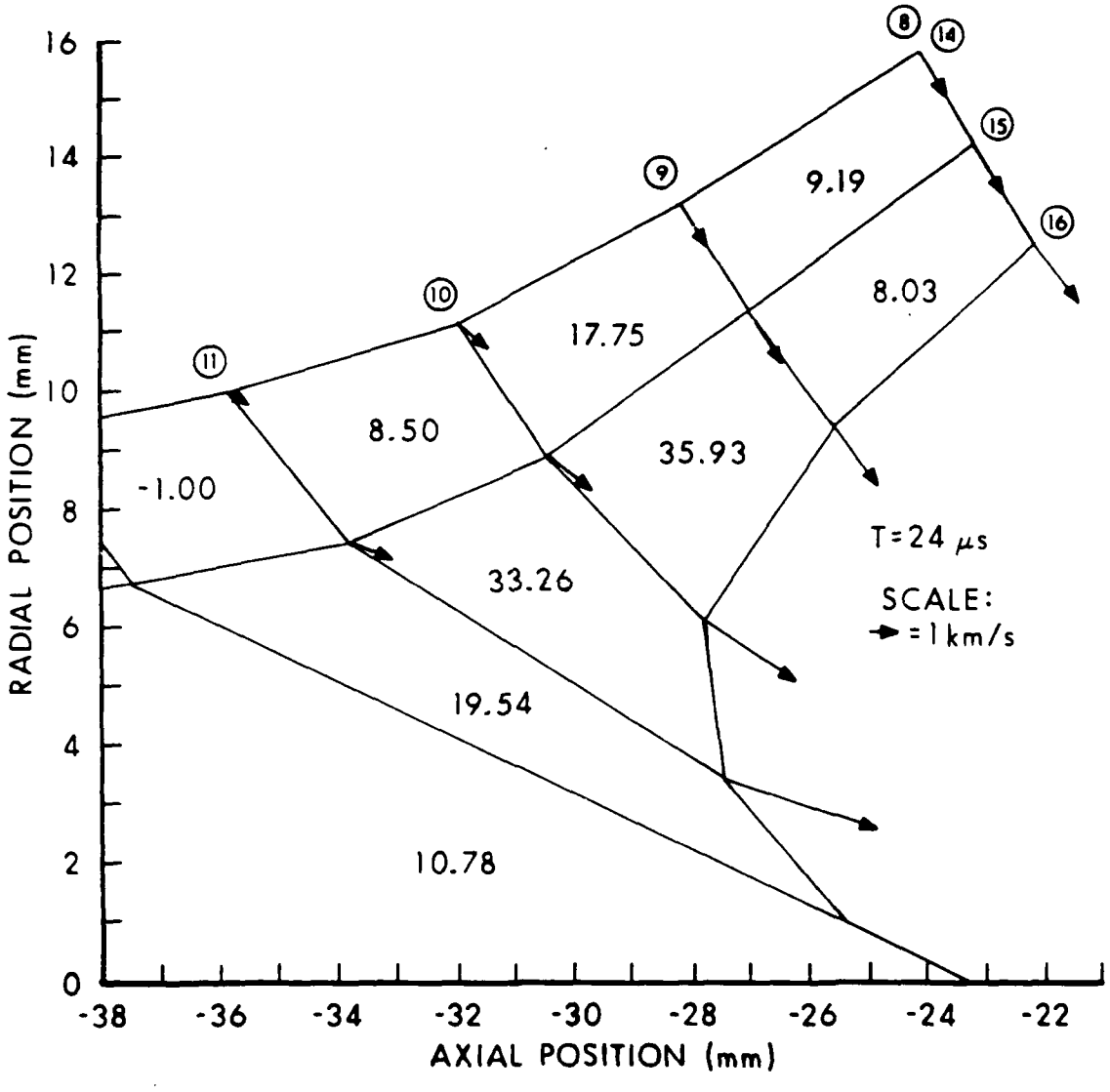

Figure 2. Cross-secion in the upper half-plane of the HEMP computational grid simulating the explosively-driven collapse of a conical shell.

III. THE ASSUMPTIONS AND RESULTS OF THE PREVIOUS STEADY-STATE JET-FORMATION THEORY

The original analysis of jet formation from a collapsing wedge, the Birkhoff, MacDougall, Pugh, and Taylor (BMPT) theory, was based on the premise that, for steady flow conditions, the process was equivalent to a diverted flow issuing from a moving collision point. This process is illustrated in Figure 3, taken from the BMPT paper, Reference 1. Figure 3a shows the formation of a jet and slug from a wedge-shell whose sides collapse with constant velocity V_o, driven by the detonation of a charge of high explosive that was in contact with its outer surface. The solid lines in Figure 3a show the collapse conditions at one instant of time and the dotted lines show the conditions at a later instant. Figure 3b shows the formation of jet and slug by the wedge-shell shown in Figure 3a from the viewpoint of an observer stationed at the moving junction A.

The high pressures involved in the process far exceed the mechanical strength of the metal in the shell, so this material was assumed to behave like a perfect fluid.* To eliminate the complexity of pressure waves and because the metal of the shell is not very compressible, the fluid was considered to be incompressible. The flow of material through the collision region was determined by applying the laws of conservation of linear momentum, mechanical energy, and mass at the boundaries of the collision region.

In BMPT theory, the constant velocity of the wedge wall, $\vec{V}_o$, is resolved into a "flow" component, $\vec{V}_F$, along the wall and a "stagnation point" component, $\vec{V}_{sp}$, along the axis of symmetry of the shell. In the reference frame of the collision region, traveling down the axis of symmetry with $\vec{V}_{sp}$, the collapse velocity is the same along each streamline.** In terms of the collapse angle, β, and the y- and x-components of the collapse velocity, V_{oy} and V_{ox}, respectively, the magnitude of the flow velocity is

$$V_F = V_{oy} \csc \beta , \tag{3.1}$$

while the stagnation point velocity of the moving junction A has a magnitude given by

$$V_{sp} = V_F \cos\beta + V_{ox}. \tag{3.2}$$

In the stationary frame of reference, the jet velocity magnitude, V_j is

$$V_j = V_F + V_{sp} \tag{3.3}$$

*A perfect fluid is non-viscous and non-conducting.

**A streamline maps the direction of the velocity at every point in space at any instant. The paths of the fluid particles are tangent to the streamlines at any instant.

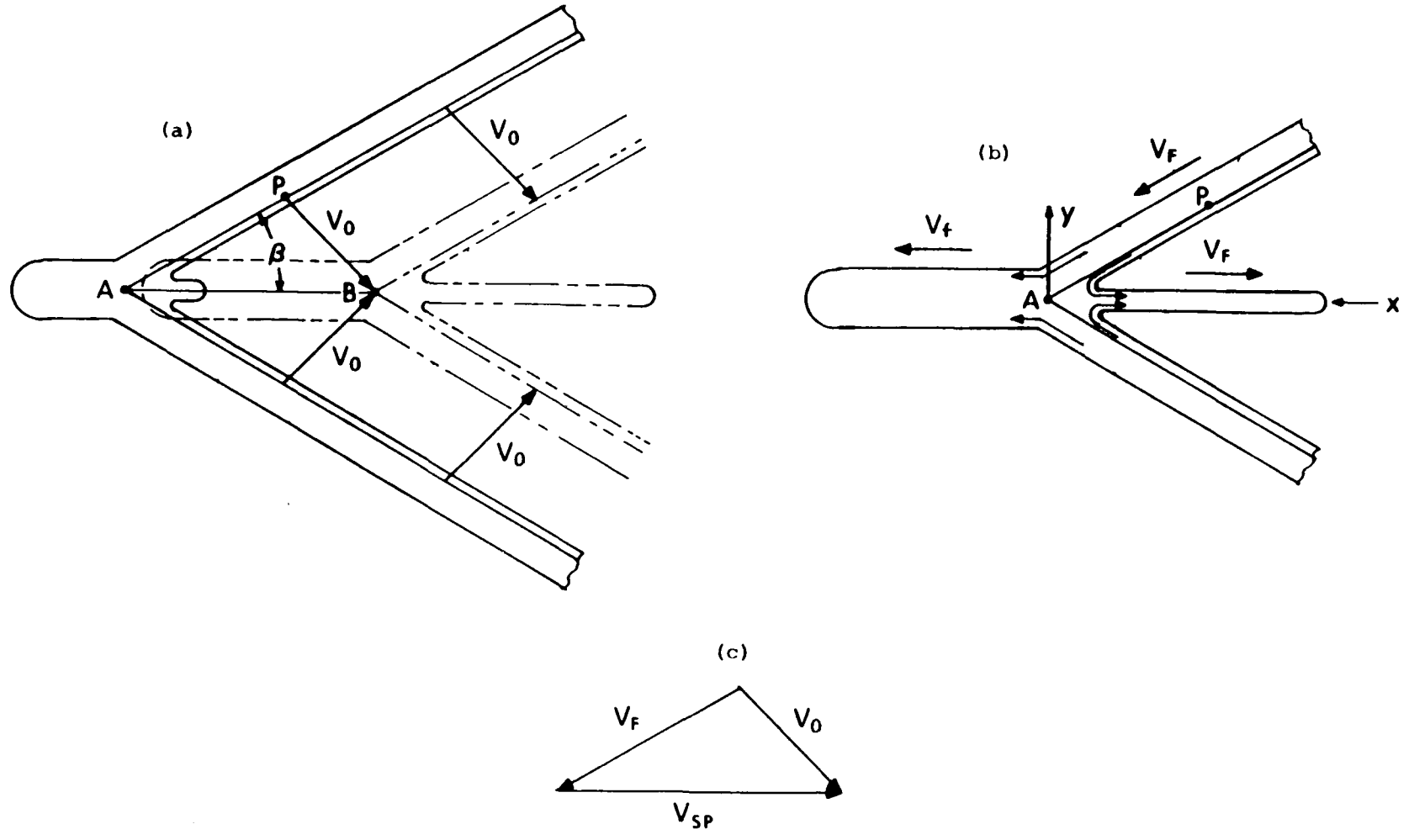

Figure 3. Formation of jet and slug from the collapse of a wedge shell; (a) from the point of view of a stationary observer, (b) as seen by an observer moving with the junction A. The vector decomposition of the collapse velocity V_o into the flow velocity V_F and the stagnation point velocity V_{sp} is shown in (c).

since the jet flow "turns the corner" and proceeds in the same direction that the stagnation point is moving. The magnitude of the slug velocity, V_s, is

$$V_s = V_{sp} - V_F, \tag{3.4}$$

since the slug flow is opposite to the stagnation point motion. The mass partition into jet mass, m_j, and slug mass, m_s, of the incoming liner (shell) mass, m_l, is

$$\frac{m_s}{m_l} = \cos^2 (\beta/2) \tag{3.5}$$

and

$$\frac{m_j}{m_l} = \sin^2 (\beta/2) \tag{3.6}$$

The conclusions reached through this analysis were considered applicable to jets produced from both conical shells and wedge shells. In the absence of convergence velocity gradients, the same results can be derived for conical geometry, by distorting the geometry somewhat to mask the essentially divergent nature of the flow. In the next section, the equivalent theory for a conical geometry is developed, under the assumption of "convergenceless flow," in order to lay the foundations for the new theory which explicitly addresses the convergence effect.

IV. JETS FROM CONVERGENCELESS CONE COLLAPSE

In order to approximate the conditions required for the application of the steady-state, BMPT, wedge-jet theory to a collapsing conical shell, the thickness and collapse velocity of the shell are assumed to be adjusted so that the collision region moves with constant velocity down the axis of symmetry of the cone and the mass entering the collision region is constant. Then, from a reference frame in the collision region, the incoming and outgoing flows are steady.*

The conditions of the liner collapse are illustrated schematically in Figure 4. Half the metal liner is shown in cross-section at the top of the figure along with the charge of high explosive. At the bottom of the figure, the conical liner is shown partially collapsed with a small amount of undetonated explosive still remaining at the end of the charge.

*The flow is steady if there is no variation with time in either the magnitude or the direction of the velocity at any stationary point in the space through which the fluid flows.

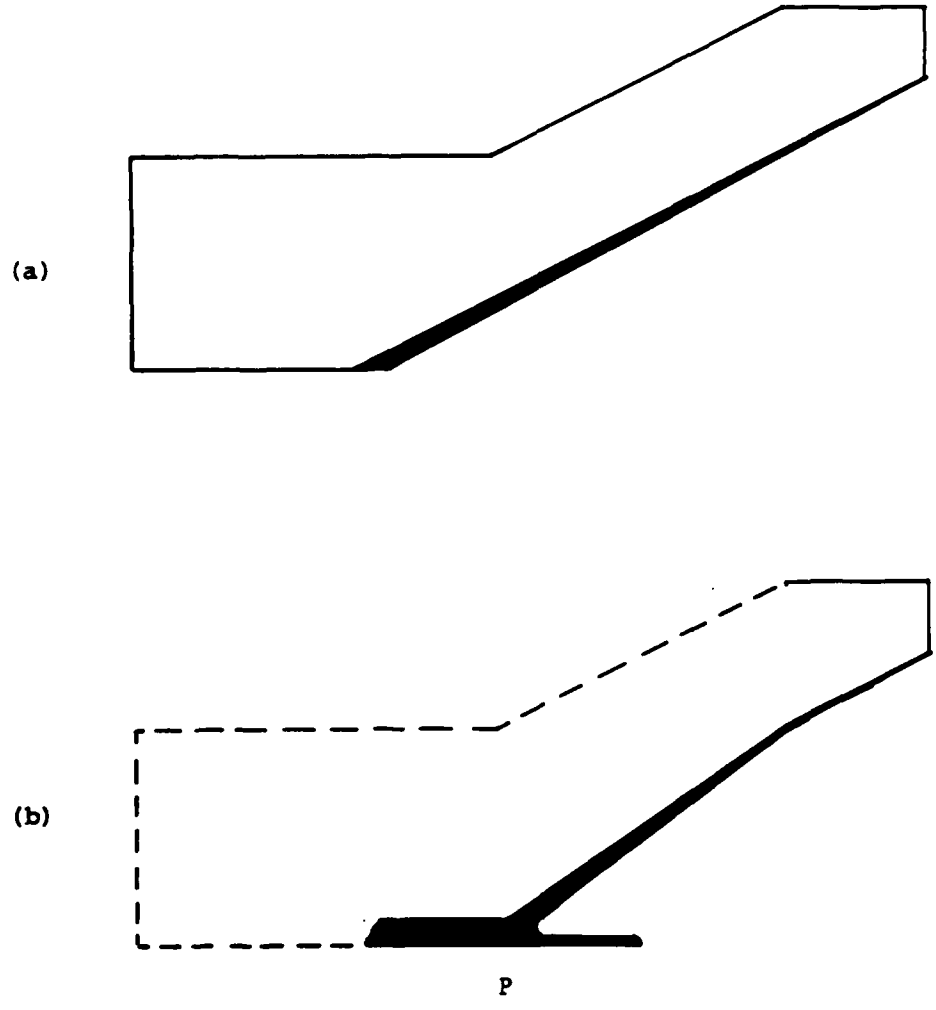

Figure 4. Schematic diagram of "constant-velocity" shaped charge with tapered conical shell liner; (a) before detonation of the high explosive, (b) with the explosive partially detonated.

The collapse conditions are such that the collapse angle β, measured with respect to the central streamline of the incoming flow, remains constant. Since an individual liner segment swells as it approaches the axis of symmetry, the incoming flow is no longer uniform,* as it was in the case of the wedge flow. The incoming flow is divergent as it approaches P and the separating streamlines have relative velocities with respect to each other. A convergence velocity gradient necessarily exists which will be neglected in the analysis of this section.

Figure 5a shows the areas intercepted by the flow on an imaginary surface enclosing the jet-formation region. Figure 5b shows the boundaries of a "quasi-uniform" flow through the formation region, reminiscent of wedge flow. The incoming flow is represented as parallel flow because constant velocity divergent flow raises many of the same complications associated with the actual flow to be treated later. The adjustment in the apparent "thickness" of the flow brought about by the convergence of the mass in the conical shell and the consequent rearrangement of the spacing between streamlines occurs in this "convergenceless" model in the interior of the collision region and is "invisible" at the boundaries.

In Figure 5b, let CE = a be the initial thickness of the flow as it enters through the bounding surface. Since the flow is axisymmetric, the total area of the boundary surface intersected by the flow is the area of a ribbon of width a and length $2\pi\bar{r}$,

$$A_o = 2\pi\bar{r}a = \pi(r_C + r_E)a \tag{4.1}$$

on the same diagram, let FG = a_1, and BA = a_2 be the radii of the deflected flows. The boundary surface areas intersected by these flows are

$$A_1 = \pi a_1^2 \tag{4.2}$$

and

$$A_2 = \pi a_2^2 \tag{4.3}$$

In the reference frame of the moving collision region, the incoming momentum per unit length of quasi-uniform flow has a z-component given by

$$p_z^{in} = -\int_{o(c)}^{a(E)} \rho(V_F\cos\beta)\ 2\pi(r_C - \varepsilon x)\ dx$$

$$= -2\pi\rho V_F \cos\beta\ (r_C a - \varepsilon a^2/2), \tag{4.4}$$

*The flow is uniform if all streamlines remain parallel to one another.

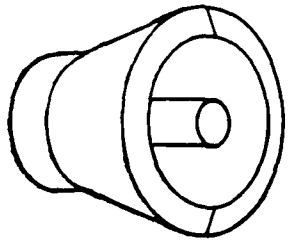

(a)

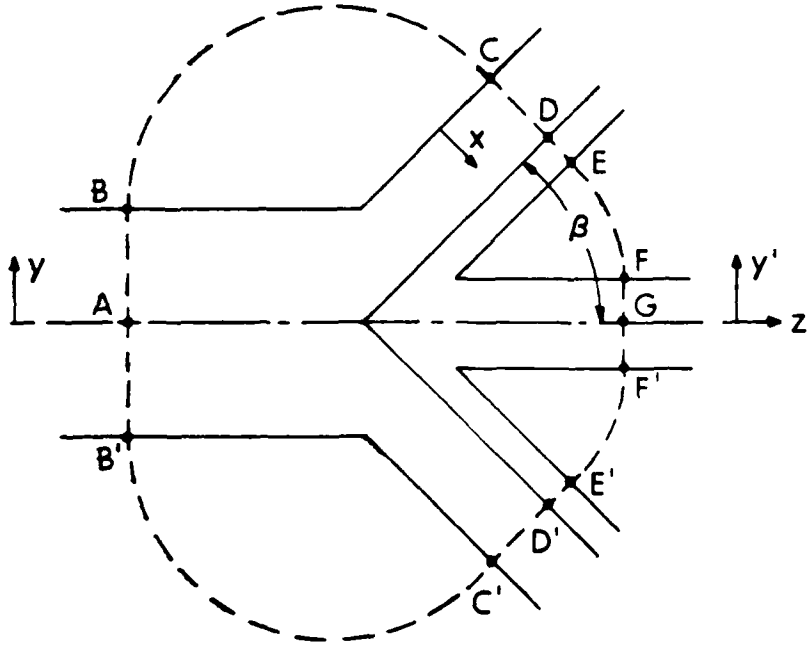

(b)

Figure 5. (a) Bounding surface for conical geometry, (b) cross-sectional view.

where x is a coordinate which measures the thickness of the flow as indicated in Figure 5b, V_F is the magnitude of the flow velocity,

$$\varepsilon = (r_C - r_E)/a, \tag{4.5}$$

ρ is the mass density of the shell material, β is the collapse angle defined by an incoming streamline and the axis of symmetry, and p_z^{in} is directed along the negative z-axis.

The outgoing momentum per unit length has a z-component of the form:

$$p_z^{out} = -\int_{o(A)}^{a_2(B)} \rho V_F 2\pi y dy + \int_{o(G)}^{a_1(F)} \rho V_F 2\pi y' dy' \tag{4.6}$$

where y and y' are indicated in Figure 5b. For continuous, incompressible flow, the relation between a, a_1 and a_2 is

$$\rho\pi(r_C + r_E)a = \rho\pi a_2^2 + \rho\pi a_1^2$$

so

$$a_1 = \sqrt{(r_C + r_E)a - a_2^2} \quad . \tag{4.7}$$

Then

$$p_z^{out} = -2\pi\rho V_F \left[a_2^2 - (r_C + r_E)a/2\right] . \tag{4.8}$$

If linear momentum is conserved in the collision frame,

$$\cos\beta\,(r_C a - \varepsilon a^2/2) = a_2^2 - (r_C + r_E)\ a/2, \tag{4.9}$$

and

$$a_2^2 = (r_C + r_E)\,\frac{a}{2}\,(\cos\beta + 1)$$

$$= (r_C + r_E)a\cos^2(\beta/2) \tag{4.10}$$

The fraction of the mass in the incoming flow which goes into the "slug" is then

$$\frac{m_s}{m_1} = \frac{a_2^2}{a\,(r_C + r_E)} = \cos^2(\beta/2) \ , \tag{4.11}$$

which is the same result obtained in BMPT theory for the slug from the collapse of a wedge shell. The mass partition in the jet is

$$\frac{m_j}{m_1} = \frac{m_1 - m_s}{m_1} = \sin^2 (\beta/2). \qquad (4.12)$$

The velocity of the slug portion of the mass will be $V_{sp} - V_F$; that of the jet mass will be $V_{sp} + V_F$, as indicated in Figure 3b.

This jet-formation model, which ignores convergence effects, gives a good qualitative description of the jets produced by the collapse of conical shells. When the effect of a time varying collapse velocity and collapse angle is incorporated by simply changing the input conditions to the steady-state model, the description is so good that, in the first examination of the validity of the model, the predicted and experimentally - determined jet characteristics were shown to agree within the precision of the experimental data[3]. Later, when a more sensitive analytic approach was taken using refined experimental data[4], small systematic deviations between predicted and observed properties were detected, but no theoretical explanation for the effects was offered. In the next section, the influence of a convergence-type velocity gradient on the mass and velocity partition in wedge-jet formation is investigated. Small, but systematic, deviations from the results of the BMPT theory are shown to occur. The derived formulae, although artificial, illustrate the changes in the jet properties with the least mathematical complexity.

V. THE INFLUENCE OF A CONVERGENCE-TYPE VELOCITY GRADIENT ON THE MASS AND VELOCITY PARTITION IN DEFLECTED WEDGE-FLOW

The effect of a velocity gradient on jet formation in the stagnation-point frame of reference is most easily assessed by using the wedge-flow model first proposed by Birkhoff, MacDougall, Pugh and Taylor. The advantage of this model is its particularly simple flow pattern.

In Figure 6, one half the cross-section through the flow and bounding surface is shown. The initial thickness of the wedge flow is CE = a, and the thicknesses of the deflected forward and rearward flows are FG = a_1 and BA = a_2, respectively. The velocity gradient across the incoming flow is assumed to be linear, in particular

$$V_F(x) = V_{OF} + \alpha x \qquad 0 \leq x \leq a \qquad (5.1)$$

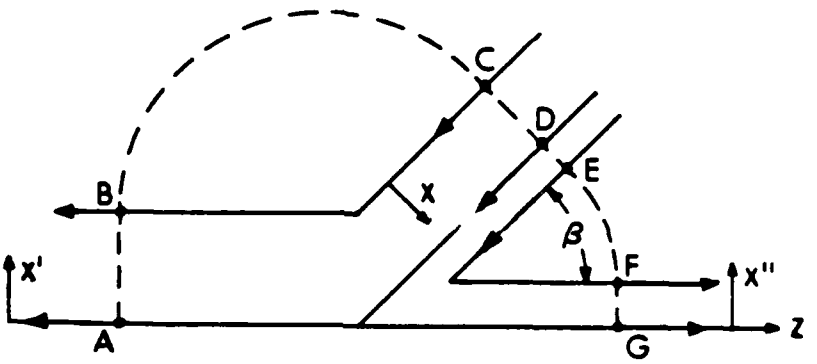

Figure 6. Flow configuration for wedge with velocity gradiant.

where V_F is the magnitude of the flow velocity at position x, measured across the thickness, with x = 0 being point C on Figure 6. V_{OF} is the flow velocity at C and

$$\alpha = (V_E - V_C)/a \tag{5.2}$$

is the "strength" of the velocity gradient.

Since the flow is assumed to be uniform and steady, there is a smooth division of the streamlines in the collision region and the incoming velocity gradient is preserved in the exiting flows.

The incoming momentum, through a surface CE across the cross-section of the flow and extending for unit length perpendicular to the plane of Figure 6, has an average z-component given by

$$\langle p_z^{in} \rangle = -\rho a \langle V_F \rangle \cos \beta, \tag{5.3}$$

where $\langle V_F \rangle$ is the average flow speed* defined by

$$\langle V_F \rangle \equiv \frac{\int_A V_{FN}\, dA}{A} \tag{5.4}$$

V_{FN} being the component of the flow velocity normal to the area element dA.

Then, since the surface CE is normal to the flow

$$\langle p_z^{in} \rangle = -\rho a \cos\beta \int_o^a \frac{V_F}{a}(x)\, dx$$

$$= -\rho \cos\beta \,(V_{OF} a + \alpha a^2/2) \tag{5.5}$$

The incoming mass per unit time is $\rho a \langle V_F \rangle$. The outgoing average momentum has the z-component,

$$\langle p_z^{out} \rangle = -\rho a_2 \langle V_{F2} \rangle + \rho a_1 \langle V_{F1} \rangle, \tag{5.6}$$

*This definition is given, for example, by Jerzy A. Owczarek in Introduction to Fluid Mechanics, (International Text Book Company, Scranton, 1968), p. 183.

where $\langle V_{F2} \rangle$ is the average flow speed into the slug, of thickness a_2, through the surface AB, and $\langle V_{F1} \rangle$ is the average flow speed into the jet, of thickness a_1, through the surface FG. Thus

$$\langle p_z^{out} \rangle = -\int_o^{a_2} \rho V_F(x')dx' + \int_o^{a_1} \rho V_F(x'')dx'' ,$$

where the integrations are performed over the surfaces whose cross-sections are AB and FG, respectively.

For this idealized deflected flow, the velocity gradients are

$$V_F(x') = V_{OF} + \alpha(a_2 - x'), \tag{5.7}$$

and

$$V_F(x'') = V_{OF} + \alpha(a_2 + x''). \tag{5.8}$$

Therefore,

$$\langle p_z^{out} \rangle = \rho \left(-V_{OF}a_2 - \frac{\alpha}{2} a_2^2 + V_{OF}a_1 + \alpha a_1 a_2 + \frac{\alpha}{2} a_1^2 \right). \tag{5.9}$$

The expression for the continuity of the flow is

$$a \langle V_F \rangle = a_1 \langle V_{F_1} \rangle + a_2 \langle V_{F_2} \rangle , \tag{5.10}$$

where

$$\langle V_{F_1} \rangle = \int_o^{a_1} \frac{V_F(x'')}{a_1} dx'' = V_{OF} + \alpha a_2 + \frac{\alpha}{2} a_1 , \tag{5.11}$$

and

$$\langle V_{F_2} \rangle = \int_0^{a_2} \frac{V_F(x')}{a_2}\, dx' = V_{OF} + \frac{\alpha}{2} a_2. \tag{5.12}$$

Then since,

$$\langle V_F \rangle = \int_0^{a} \frac{V_F(x)}{a}\, dx = V_{OF} + \frac{\alpha}{2} a, \tag{5.13}$$

$$V_{OF} a_1 + \alpha a_1 a_2 + \frac{\alpha}{2} a_1^2 = V_{OF} a + \frac{\alpha}{2} a^2 - V_{OF} a_2 - \frac{\alpha}{2} a_2^2 \tag{5.14}$$

Since momentum is conserved,

$$a \cos\beta\, (V_{OF} + \alpha a/2) = 2a_2\, (V_{OF} + \alpha a_2/2) - a(V_{OF} + \alpha a/2). \tag{5.15}$$

The thickness of the outgoing flow is then

$$a_2 = \frac{-V_{OF}}{\alpha} \pm \frac{\sqrt{V_{OF}^2 + \alpha a\, (\cos\beta + 1)\, (V_{OF} + \alpha a/2)}}{\alpha}, \tag{5.16}$$

where the limitation

$$0 \leq a_2 \leq a$$

determines the root to be chosen. Note that, if Equation (5.16) is expanded by means of the binomial theorem, the result is

$$a_2 = a \cos^2(\beta/2) + \frac{\alpha a^2}{2V_{OF}} \cos^2(\beta/2) + \cdots \tag{5.17}$$

in agreement with BMPT theory if $\alpha = 0$. For constant influx energy (see Appendix A), as α increases, V_{OF} decreases until finally, the limiting value for V_{OF} non-negative is $a_2 = a \cos(\beta/2)$.

As one would expect from a velocity gradient of the sort assumed (with $\alpha > 0$), less mass is required in the jet to balance the axial momentum in the stagnation point frame of reference because the average flow velocity in the jet, $\langle V_{F1} \rangle$, is greater then the average flow velocity in the slug, $\langle V_{F2} \rangle$. Some examples of the phenomenon are shown in Table I.

Table I. Dependence of Wedge-Flow on Velocity Gradient For Constant Influx Energy in Stagnation Point Frame

$V_{OF} = 2.751$ km/s $a = 4.624$mm $\beta = 36.4$ degrees

α (km/s/mm)	V_{OF} (km/s)	a_1 (mm)	a_2 (mm)	$\langle V_{F1} \rangle$ (km/s)	$\langle V_{F2} \rangle$ (km/s)
0.0	2.751	0.451	4.173	2.751	2.751
0.1	2.516	0.419	4.205	2.957	2.726
0.2	2.276	0.391	4.233	3.162	2.699
0.3	2.028	0.365	4.259	3.361	2.667
0.4	1.774	0.342	4.282	3.555	2.630
0.5	1.513	0.321	4.303	3.745	2.589
0.6	1.245	0.302	4.322	3.929	2.542
0.8	0.685	0.267	4.357	4.277	2.428
1.0	0.093	0.236	4.388	4.599	2.287
1.2	-.537	0.207	4.417	4.887	2.113
1.4	-1.218	0.177	4.447	5.132	1.895

VI. JETS FROM COLLAPSING CONICAL SHELLS

The steady flow associated with a collapsing conical shell is non-uniform. This introduces additional complication into its analysis.

According to Sterne's theory of the collapsing cylindrical shell, the radial velocity of the central streamline is essentially unaffected by the internal pressures until the collapse is nearly complete. Consequently, the other streamlines diverge from this streamline and the central streamline is a natural point of reference in the flow analysis.

In the following it is assumed that, in a reference frame in which this streamline is at rest, the flow pattern appears stationary. This conical flow pattern is illustrated in Figure 7 along with the flow velocities as seen in the "stagnation point" reference frame of the central streamline.

A boundary region, indicated by the dashed line in Figure 7, is established just outside the high pressure collision region whose existence was indicated in Figure 2. The flow velocities are obtained by resolving the collapse velocities along their respective streamlines. The reference frame velocity is the axial component of the collapse velocity on the central streamline, evaluated at the point where the streamline first intercepts the surface of integration, just above the collision region. The collapse velocities of the other streamlines have different axial components, since they are diverging from the central one.

The momentum of the fluid entering the dotted boundary surface, illustrated in Figure 7, will be conserved. As in the previous analysis of conical flow, CE = a is the thickness of the incoming flow and the projected area of the flow on the boundary surface is $A_o = \pi(r_C + r_E)\, a$, where r_C and r_E are radii to the boundary points C and E in Figure 7. The radii of the outgoing "jet" and "slug" flows are a_1 and a_2, respectively. The projected areas of the outgoing flows on the boundary surface are $A_1 = \pi a_1^2$, for the jet, and $A_2 = \pi a_2^2$ for the slug.

Let x label the position of a streamline in the incoming flow and let $V_{FN}(x)$ be the velocity component of the incoming flow at x normal to the boundary surface. It is assumed that the velocity gradient of this normal flow is linear, i.e.,

$$V_{FN}(x) = V_{OFN} + \alpha x \qquad 0 \leq x \leq a \qquad (6.1)$$

where V_{OFN} is the normal component of the flow velocity at point C in Figure 7, and x is measured from point C. The velocity components parallel to the boundary CE are associated with the "natural" streamline divergence and are neglected in the analysis of the collision.

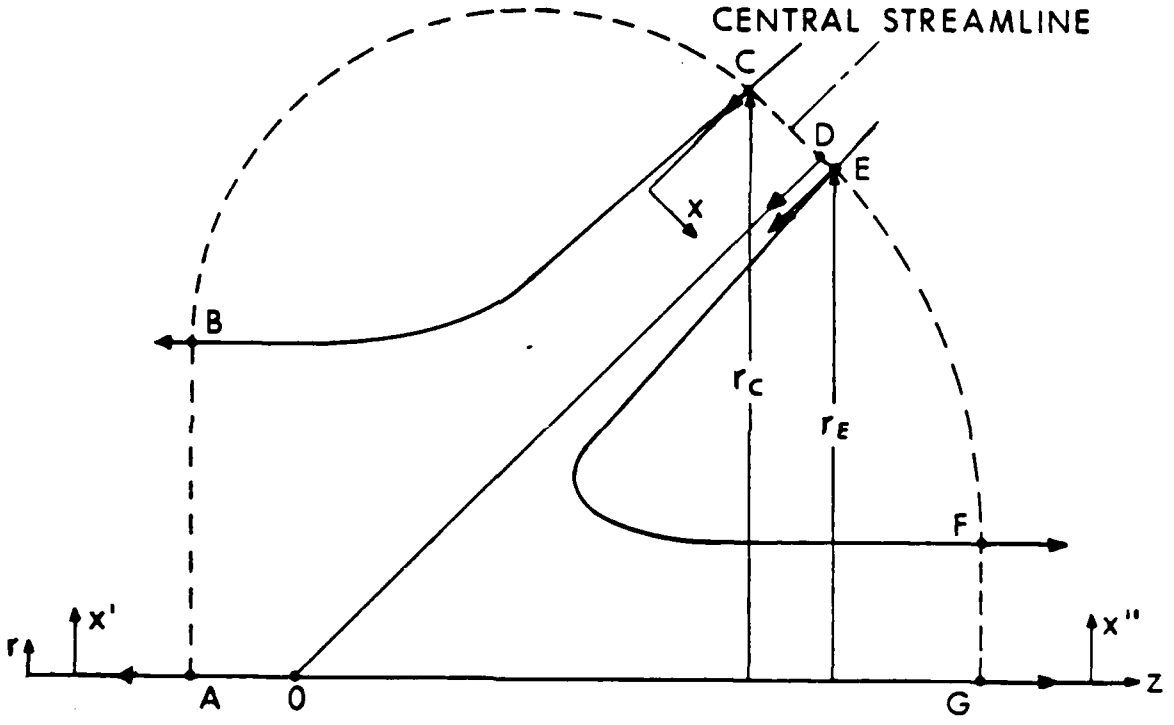

Figure 7. Flow conf uration for steady, non-uniforms flow for evaluation of velocity distribution.

The average momentum per unit length of the flow entering through the boundary surface has a z-component, $\langle p_z^{in} \rangle$, given by

$$\langle p_z^{in} \rangle = -\rho \langle V_{FN} \rangle A_c \cos \beta, \tag{6.2}$$

where

$$\langle V_{FN} \rangle = \frac{1}{A_o} \int_o^a V_{FN}(x)\, 2\pi\, (r_c - \varepsilon x)\, dx. \tag{6.3}$$

The integrated incoming momentum, in the negative z-direction, is

$$\langle p_z^{in} \rangle = -2\pi\rho\, F(a) \cos \beta\ , \tag{6.4}$$

where $$F(a) \equiv r_c a\, V_{OFN} + (\alpha r_c - \varepsilon V_{OFN})\, a^2/2 - \alpha\varepsilon a^3/3. \tag{6.5}$$

The average momentum leaving the bounding surface has a z-component, $\langle p_z^{out} \rangle$, given by

$$\langle p_z^{out} \rangle = -\int_{o(A)}^{a_2(B)} \rho V_F(x') 2\pi x' dx' + \int_{o(G)}^{a_1(F)} \rho V_F(x'') 2\pi x'' dx''\ , \tag{6.6}$$

where $V_F(x')$ and $V_F(x'')$ are the streamline flow velocities in the slug (x') and jet (x'') respectively. These flows are normal to the boundary surfaces.

It is assumed that the normal components of the individual streamlines are preserved in this "perfect" collision. The spacing between the streamlines changes due to convergence effects. For continuous incompressible flow, conservation of mass demands that

$$a(r_c + r_E) \langle V_{FN} \rangle = a_1^2 \langle V_{F_1} \rangle + a_2^2 \langle V_{F_2} \rangle \tag{6.7}$$

where $$\langle V_{FN} \rangle = \frac{2F(a)}{a\,(r_c + r_E)} \tag{6.8}$$

$$\langle V_{F_1} \rangle = \frac{2}{a_1^2} \int_o^{a_1} V_F(x'') x'' dx'' \tag{6.9}$$

and $$\langle V_{F_2} \rangle = \frac{2}{a_2^2} \int_o^{a_2} V_F\,(x') x' dx' \tag{6.10}$$

Then, the expression for continuity is

$$F(a) = \int_0^{a_1} V_F(x'')x''dx'' + \int_0^{a_2} V_F(x')x'dx' \tag{6.11}$$

Let

$$I_1 \equiv \int_0^{a_1} V_F(x'')x''dx'' \tag{6.12}$$

$$= F(a) - \int_0^{a_2} V_F(x')x'dx',$$

then

$$\langle V_{F1} \rangle = \frac{2I_1}{a_1^2} \tag{6.13}$$

The axial component of the average momentum is therefore

$$\langle p_z^{out} \rangle = -2\pi c \left\{ 2\int_0^{a_2} V_F(x')x'dx' - F(a) \right\}. \tag{6.14}$$

Since momentum is conserved,

$$\pi(a)\cos\theta = 2\int_0^{a_2} V_F(x')x'dx' - F(a) \quad , \tag{6.15}$$

or

$$\frac{1}{2}(1 + \cos\theta)\, F(a) = \int_0^{a_2} V_F(x')x'dx'. \tag{6.16}$$

Let

$$I_2 \equiv \int_0^{a_2} V_F(x')x'dx', \tag{6.17}$$

then

$$\langle V_{F2} \rangle = \frac{2I_2}{a_2^2} .$$

In order to evaluate the integral I_2, the velocity distribution in the exiting flow, $V_F(x')$, must be determined from the spacing between streamlines in the slug flow. Figure 8 shows the flow variables considered.

Let a_2^* be the lagrangian label of the streamline which divides the jet-slug flow. The area of a streamtube* in the incoming slug flow is then

$$A_y = \pi y \, (r_{a_2^*} + r_y), \qquad 0 \leq y \leq a_2^* \tag{6.18}$$

where A_y is the area between the dividing streamline, a_2^*, and the streamline with coordinate y; $r_{a_2^*}$ is the radial position of the point a_2^* on the boundary surface and r_y is the radial position of the point y on this same surface. Let the bounding surface CE be normal to the central streamline of the flow.

If θ is the angle between the line CE and the positive z-axis in Figure 8, then

$$\sin\theta = \frac{r_C - r_E}{a} \quad \frac{r_y - r_{a_2^*}}{y} \tag{6.19}$$

and also

$$\frac{r_C - r_{a_2^*}}{a_2^*} = \frac{r_C - r_E}{a} \tag{6.20}$$

so

$$r_{a_2^*} = r_C - \varepsilon a_2^* \tag{6.21}$$

*A streamtube is a tube in the flow velocity field filled with the flowing fluid and formed by all the streamlines passing through a closed curve defining the circumference of a cross-section of the tube.

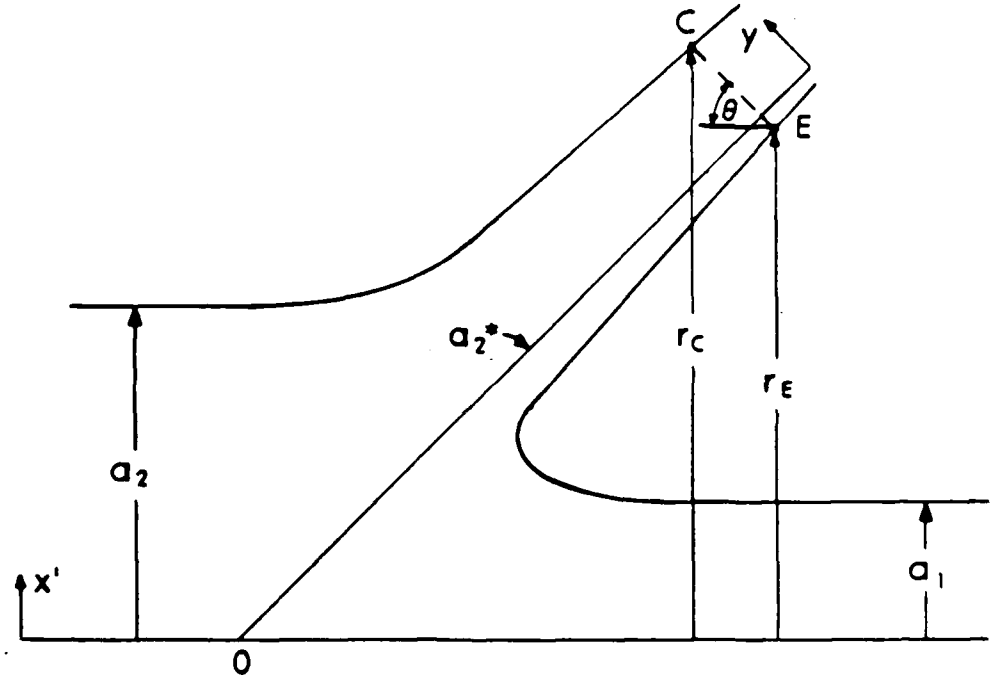

Figure 8. Flow configuration for steady, non-uniform flow for evaluating streamline spacing.

where ε is given by Equation (4.5). The area between any two streamlines is then

$$A_y = \pi y \, (2r_c - 2\varepsilon a_2^* + \varepsilon y). \tag{6.22}$$

All these streamlines are carried into the slug, where the spacing is determined by the area $A_{x'}$ of the stream tube, where

$$A_{x'} = \pi x'^2. \tag{6.23}$$

Since the flow is incompressible, $A_{x'} = A_y$ and, since y is positive,

$$y = \frac{-(r_c - \varepsilon a_2^*)}{\varepsilon} + \frac{\sqrt{(r_c - a_2^*)^2 + \varepsilon x'^2}}{\varepsilon} \tag{6.24}$$

Mapping the streamline velocities from one configuration of the flow, $V_F(y)$ incoming, to the other, $V_F(x')$ outgoing, leads to the transformation

$$V_F(y) = V_F(a_2^*) - \alpha y = V_{OFN} + \alpha a_2^* - \alpha y \tag{6.25}$$

Letting $A(a_2^*) \equiv r_c - \varepsilon a_2^*$, it follows that

$$V_F(x') = V_{OFN} + \alpha a_2^* + \frac{\alpha}{\varepsilon} A(a_2^*) - \frac{\alpha}{\varepsilon}\sqrt{A^2(a_2^*) + \varepsilon x'^2} \quad . \tag{6.26}$$

Substituting for $V_F(x')$ in Eq. (6.17) for the integral I_2 and integrating gives

$$I_2 = \frac{V_{OFN}}{2} a_2^2 + \frac{\alpha r_C}{2\varepsilon} a_2^2 - \frac{\alpha}{3\varepsilon^2}\left[(r_C - \varepsilon a_2^*)^2 + \varepsilon a_2^2\right]^{3/2} + \frac{\alpha}{3\varepsilon^2}(r_C - \varepsilon a_2^*)^3 \quad . \tag{6.27}$$

The result of equating the incoming and outgoing "slug" areas is that

$$a_2^* = \frac{r_C - \sqrt{r_C^2 - \varepsilon a_2^2}}{\varepsilon} \quad , \tag{6.28}$$

so

$$I_2 = \frac{1}{2} V_{OFN} a_2^2 + \frac{1}{2} \alpha r_C a_2^2/\varepsilon - \frac{1}{3}\alpha r_C^3/\varepsilon^2 + \frac{\alpha}{3\varepsilon^2}(r_C^2 - \varepsilon a_2^2)^{3/2} \tag{6.29}$$

Now I_1 is just the difference between F(a), Eq. (6.5), and I_2. Once I_1 is known, $\langle V_{F1} \rangle$ follows from Eq. (6.13). Then $\langle V_{F2} \rangle$ can be obtained by dividing twice I_2 by a_2^2. The magnitude of the average flow velocity into the slug is then

$$\langle V_{F2} \rangle = V_{OFN} + \frac{\alpha r_C}{\varepsilon} - \frac{2\alpha}{3\varepsilon^2 a_2^2}(r_C^3 - [r_C^2 - \varepsilon a_2^2]^{3/2}) \quad . \tag{6.30}$$

The expression for conservation of the axial component of the linear momentum, Eq. (6.16), becomes

$$\frac{1}{2}(1 + \cos\beta) F(a) = \frac{1}{2}(V_{OFN} + \frac{\alpha r_C}{\varepsilon}) a_2^2 + \frac{\alpha}{3\varepsilon^2}(r_C^2 - \varepsilon a_2^2)^{3/2} - \frac{\alpha r_C^3}{3\varepsilon^2} \tag{6.31}$$

Let

$$K = \frac{1}{2}(1 + \cos\beta) F(a) + \frac{\alpha r_C^3}{3\varepsilon^2} \quad , \tag{6.32}$$

$$L = \frac{\alpha}{3\varepsilon^2} \tag{6.33}$$

and

$$M = \frac{1}{2}(V_{OFN} + \alpha r_C/\varepsilon) \, . \tag{6.34}$$

Then, Equation (6.31) becomes,

$$K - Ma_2^2 = L(r_C^2 - \varepsilon a_2^2)^{3/2}. \tag{6.35}$$

Squaring both sides, rearranging terms and letting

$$u = a_2^2 \tag{6.36}$$

$$N = \frac{M^2 - 3(L\varepsilon r_C)^2}{\varepsilon^3 L^2} \tag{6.37}$$

$$V = \frac{3L^2\varepsilon r_C^4 - 2KM}{\varepsilon^3 L^2} \tag{6.38}$$

and

$$P = \frac{K^2 - L^2 r_C^6}{\varepsilon^3 L^2} \tag{6.39}$$

the result is the cubic equation,

$$u^3 + Nu^2 + Vu + P = 0 \tag{6.40}$$

The cubic equation for the mass distribution, Eq. (6.40), is solved by the standard methods.* If

$$Q = \frac{3V - N^2}{9}, \tag{6.41}$$

$$R = \frac{9NV - 27P - 2N^3}{54}, \tag{6.42}$$

$$S = \left(R + \sqrt{Q^3 + R^2}\right)^{1/3} \tag{6.43}$$

*For example, see Murray R. Spiegel, Mathematical Handbook of Formulas and Tables, Schaum's outline series (McGraw-Hill, New York, 1968), p.32.

and

$$T = \left(R - \sqrt{Q^3 + R^2}\right)^{1/3} , \tag{6.44}$$

then the solutions to Equation (6.40) are

$$u_1 = S + T - N/3 , \tag{6.45}$$

$$u_2 = -\frac{1}{2}(S + T) - \frac{N}{3} + \frac{i\sqrt{3}}{2}(S - T) , \tag{6.46}$$

and

$$u_3 = -\frac{1}{2}(S + T) - \frac{N}{3} - \frac{i\sqrt{3}}{2}(S - T). \tag{6.47}$$

For physical reasons, $0 \leq u \leq a(r_C + r_E)$, and this criteria is used to select the proper root.

Once a_2 has been determined, by taking the positive square root of the appropriate value of u, $\langle V_{F2} \rangle$, the average flow velocity in the "slug" flow, can be obtained from Eq. (6.30). $\langle V_{F1} \rangle$, the average "jet" flow velocity, follows from Eq. (6.7), since a_1 can be determined from the area identity,

$$\frac{a_1^2}{a(r_C + r_E)} = 1 - \frac{a_2^2}{a(r_C + r_E)} . \tag{6.48}$$

Table 2 shows the results of increasing the strength of the velocity gradient, α, on the other properties of the flow in the conical geometry. For these conditions, the behavior of the flow parameters for the flow with linear convergence - velocity gradient are quite similar in character to those obtained in Section 5 for wedge flow with velocity gradient. The calculations were made for constant influx energy (see Appendix C). For $\alpha = 0$, the treatment of Section IV is used.

Table 2. Dependence of Conical-Flow Properties in Stagnation Point Frame on Velocity Gradient for Constant Influx Energy

V_{0FN} = 2.900 km/s a = 4.624 mm β = 36.4 degrees

ϵ = 0.824 r_C = 13.22 mm r_E = 9.41 mm

α (km s^{-1} mm^{-1})	V_{0FN} (kms^{-1})	a_1 (mm)	a_2 (mm)	$\langle V_{F1} \rangle$ (kms^{-1})	$\langle V_{F2} \rangle$ (kms^{-1})
0.0	2.900	3.19	9.72	2.900	2.900
0.1	2.679	3.06	9.76	3.116	2.876
0.2	2.451	2.97	9.79	3.323	2.847
0.3	2.218	2.86	9.82	3.548	2.816
0.4	1.978	2.80	9.84	3.730	2.779
0.5	1.732	2.69	9.87	3.934	2.740
0.6	1.479	2.61	9.89	4.149	2.694
0.8	0.952	2.46	9.93	4.520	2.586
1.0	0.396	2.33	9.96	4.881	2.452

VII. COMPARISON OF THE WEDGE AND CONICAL SOLUTIONS

Figure 9 illustrates the effect of varying the strength of the convergence-velocity gradient, α, on the mass partitioning in the wedge and conical flows. Both flows are constrained to have constant influx thickness, collapse angle, and kinetic energy. For the wedge flow, the ratio of the mass of the slug formed by a collapsing liner element to the mass of the element itself increases smoothly from $\cos^2(\beta/2)$ to $\cos(\beta/2)$. Above $\cos(\beta/2)$, because of the constraint of constant influx energy, the strength of the gradient can only be increased by reversing the flow direction of part of the flow, a physically unappealing situation. For the conical flow, the fraction of the mass going into the slug increases smoothly, following the wedge flow.

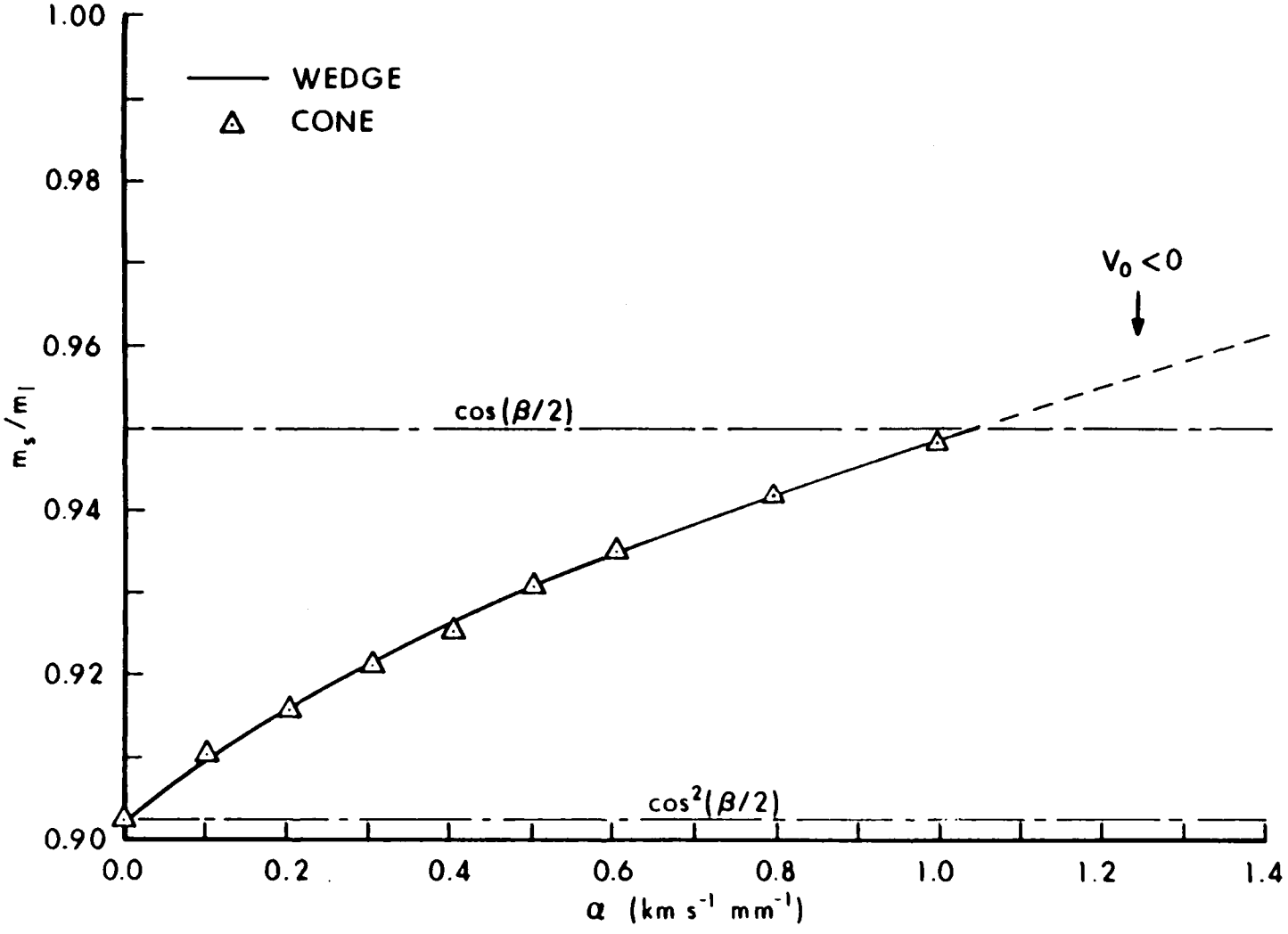

Figure 9. Behavior of mass partition as the gradient strength increases for wedge and conical flow under the condition of constant influx energy. (Triangles represent calculated values).

The physical reason for this great similarity is illustrated with the help of Figure 10. The quantity F(x) is

$$r_C V_{OFN} x + (\alpha r_C - \varepsilon V_{OFN})\, x^2/2 - \varepsilon\alpha x^3/3$$

and plays the role of an area-weighted average of the incoming velocity. As the thickness coordinate, x, is increased from 0 to a, 4.624 mm, the average velocity increases. As the strength of the velocity gradient increases, the shape of the velocity distribution changes from a curve with gradually decreasing slope, to one of constant slope, to one of increasing slope. Even for the larger values of α, under the constraints of constant influx energy and positive V_{OFN}, the contribution from the cubic term is not great and the distribution resembles the corresponding wedge distribution quantity, $f(x) = V_{OF}\, x + \alpha x^2/2$.

VIII. APPLICATION OF THE THEORY

In order to illustrate the new jet-formation analysis, the input boundary conditions from a HEMP code simulation of cone collapse will be used to calculate the properties of the jet and slug segments produced from one element of the liner. In Figure 2, the material in the segment of the cone whose cross-section in the upper half-plane is bounded by the grid lines 8, 9, 14, and 16, is assumed to collapse steadily into the jet-formation region below boundary line 9. The velocities and positions of the node points on the boundary surface just above the high-pressure collision region are given in Table 3.

Table 4 gives the flow velocities and directions, relative to the positive z-axis, of these boundary points as well as the "stagnation point" velocities for all three streamlines, as computed from Equations (3.1) and (3.2), with the appropriate changes in notation to reflect the new coordinate axes.

The "thickness" of the incoming flow, as measured normal to the central streamline, is

$$a = 4.624 \text{ mm}$$

The slope of the boundary line in the flow, as defined by Equation (4.5), is

$$\varepsilon = 0.8240,$$

where the radii to the edges of the boundary surface are

$$r_C = R(9,14) = 13.22 \text{ mm}$$

and

$$r_E = R(9,16) = 9.41 \text{ mm}.$$

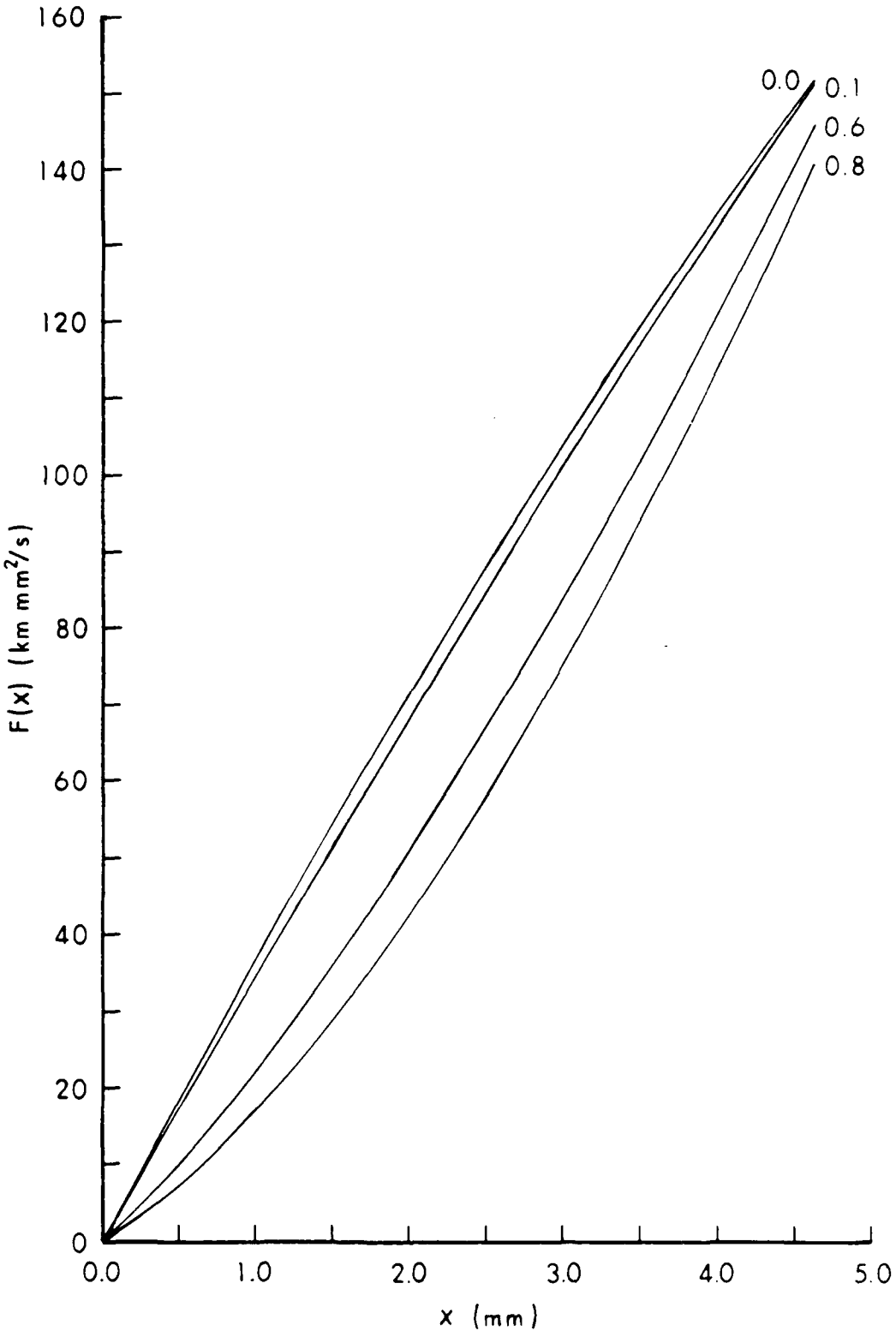

Figure 10. Area-weighted velocity distribution for various values of the strength of the velocity gradient.

Table 3. Input Boundary Conditions For The Jet-Formation Theory

Node Point	V_z (km/s)	V_r (km/s)	V (km/s)	R (mm)	Z (mm)
(9,14)	0.915	-1.478	1.738	13.22	-28.22
(9,15)	1.153	-1.803	2.140	11.40	-27.06
(9,16)	1.565	-2.185	2.688	9.41	-25.60

Table 4. Flow and Stagnation Point Velocities Computed From The Input Conditions

Node Point	V_F (km/s)	θ_F (deg)	V_{sp} (km/s)
(9,14)	2.758	32.4	3.244
(9,15)	3.038	36.4	3.598
(9,16)	3.278	41.8	4.009

In order to analyze this data with the BMPT theory, the velocity gradient and flow divergence must be ignored. Taking the central streamline to characterize the flow, the fraction of the liner mass going into the "slug" is, from Equation (4.11),

$$\frac{m_s}{m_l} = \frac{a_2^2}{a(r_C + r_E)} = \cos^2 (\beta/2) = 0.9024,$$

since β = 36.4 degrees. The radius of the slug, a_2, is 9.72 mm. The jet velocity, from Equation (3.3), is 3.038 km/s + 3.598 km/s or 6.636 km/s, while the slug velocity, from Equation (3.4), is 0.560 km/s.

Note that, in this case, the incoming kinetic energy, in the stagnation point reference frame, is expected to be 135.4 kJ/cm (if the flow had no velocity gradient).

To analyze the data with the new theory, the (linear) velocity gradient across the thickness a must be determined. The components of the flow velocities of the surface streamlines normal to the boundary surface are

$$|\overrightarrow{V_{FN}}(9,14)| = |\vec{V}_F^{\bullet}(9,14)| \cos 4^{\circ} = 2.751 \frac{km}{s} = V_{OFN}$$

and

$$|\overrightarrow{V_{FN}}(9,16)| = |\vec{V}_F(9,16)| \cos 5.4^{\circ} = 3.263 \frac{km}{s} .$$

The components of the flow velocities parallel to the boundary surface are

$$|\overrightarrow{V_{FP}}(9,14)| = - |\vec{V}_F(9,14)| \sin 4^{\circ} = - 0.192 \frac{km}{s}$$

and

$$|\overrightarrow{V_{FP}}(9,16)| = |\vec{V}_F(9,16)| \sin 5.4^{\circ} = + 0.308 \frac{km}{s}$$

These oppositely-directed velocity components are a manifestation of the flow divergence. These "lateral" velocities are ignored in the jet formation calculation.

The strength of the (normal) velocity gradient is, from Equation (5.2),

$$\alpha = 0.1107 \frac{km/s}{mm}$$

Based on the assumption of a linear velocity gradient, the predicted flow velocity on the central streamline is 2.990 km/s, about 98 percent of the input value of 3.038 km/s.

The fact that the "stagnation point" velocities of the surface streamlines differ from each other and from the stagnation point velocity of the central (reference) streamline is a consequence of the divergent flow imposed by the conical geometry. Nevertheless, for a properly-tapered conical shell, these streamlines are embedded in their same relative positions in the surface of integration as this surface translates down the axis of symmetry of the shell, so that steady flow conditions are achieved.

The key variables in the theory of conical flow are given in Table 5. The cubic equation to be solved is

$$u^3 + Nu^2 + Vu + P = 0$$

From Equations (6.41) and (6.42),

$$Q = -87.39 \times 10^{-8}\ m^4$$

and

$$R = -816.50 \times 10^{-12}\ m^6$$

Since the coefficients in the equation are real, the discriminant, $D = Q^3 + R^2$, determines the nature of the roots. In this case,

$$D = -726.2 \times 10^{-24}\ m^{12};$$

so all the roots are real and unequal. S and T are then computed from Equations (6.43) and (6.44) and are displayed in Table 6. From Equations (6.45), (6.46) and (6.47), the solutions for $u = a_2^2$ are

$$u_1 = 1.309 \times 10^{-4}\ m^2$$

$$u_2 = -26.913 \times 10^{-4}\ m^2$$

$$u_3 = 0.953 \times 10^{-4}\ m^2$$

Table 5. The Key Variables In The New Theory

Symbol	Value	Equation
K	$0.2669\ m^3/s$	(6.42)
L	$0.5435 \times 10^5\ s^{-1}$	(6.43)
M	0.2264×10^4 m/s	(6.44)
N	$24.65 \times 10^{-4}\ m^2$	(6.47)
V	$-59.62 \times 10^{-8}\ m^4$	(6.48)
P	$33.56 \times 10^{-12}\ m^6$	(6.50)

Table 6. Solutions To The Cubic Equation Defining The Mass Partition In Conical Flow

$$S_1 = 9.348 \times 10^{-4}\ m^2\ (\cos\ 59.37^\circ + i \sin\ 59.37^\circ)$$

$$S_2 = 9.348 \times 10^{-4}\ m^2\ (\cos\ 179.37^\circ + i \sin\ 179.37^\circ)$$

$$S_3 = 9.348 \times 10^{-4}\ m^2\ (\cos\ 299.37^\circ + i \sin\ 299.37^\circ)$$

$$T_1 = 9.348 \times 10^{-4}\ m^2\ (\cos\ 300.63^\circ + i \sin\ 300.63^\circ)$$

$$T_2 = 9.348 \times 10^{-4}\ m^2\ (\cos\ 180.63^\circ + i \sin\ 180.63^\circ)$$

$$T_3 = 9.348 \times 10^{-4}\ m^2\ (\cos\ 60.63^\circ + i \sin\ 60.63^\circ)$$

Since u must satisfy

$$o \leq u \leq 1.046 \times 10^{-4}\ m^2,$$

$$a_2^2 = 0.953 \times 10^{-4}\ m^2$$

The radius of the slug is 9.76 mm and the mass division is such that

$$\frac{m_s}{m_1} = \frac{a_2^2}{a(r_C + r_E)} = 0.9101$$

The average jet velocity is the sum of the stagnation point velocity of the central streamline, 3.598 km/s, and the average flow velocity into the jet in the stagnation point reference frame, obtained from Equation (6.9), 3.232 km/s. The result is an average jet velocity of 6.830 km/s. The average slug velocity is the difference between the reference frame velocity and the average flow velocity into the slug obtained from Equation (6.10), 2.969 km/s. The result is 0.629 km/s.

Note that, in this case, the incoming kinetic energy, in the stagnation point reference frame, is 131.8 kJ/cm.

IX. COMPARISON WITH EXPERIMENT

The small, systematic deviations between theory and experiment discovered by Eichelberger* will now be discussed. His experimental observations were of liner mass, jet velocity, and slug mass. The liner was

*Reference 4, p. 402.

divided into sections, and the slugs corresponding to different liner segments were recovered by firing the shaped charge into a reservoir of water. The results of such experiments with a particular charge are shown in Figure 11. The jet mass was estimated by subtracting the observed slug mass from the observed cone segment mass.

The collapse angle β as a function of liner segment position was estimated by means of the slug mass measurements and the relation

$$\frac{dm_s}{dm} = \cos^2 (\beta/2) \qquad (9.1)$$

where m_s is the mass of the slug and m is the mass of the parent liner segment. Equation (9.1) is the differential form of Equation (3.5). The experimental curve of m_s verus m (Figure 11) was fit using Birge's method[8] to a polynomial which was subsequently differentiated to obtain the values of β displayed in Figure 12. The coordinate x is measured from the apex of the cone, along the axis of symmetry, to a point at which a perpendicular is erected to the liner wall. Note that, according to the new theory, the mass of the slug is no longer determined solely by the mass of the liner and the collapse angle.

The rapid variation in β, especially near the base of the liner, indicates that the collapse of this shaped-charge is non-steady. Pugh, Eichelberger and Rostoker*, PER, deduced a formula for the shape of a conical liner collapsing with a velocity gradient along its length (instead of through its thickness). The determination of the jet-formation conditions, the collapse velocity V_o and the collapse velocity gradient, dV_o/dx, was relatively complicated, but the jet formation itself was treated by the steady-state theory. Therefore, any discrepancies found between the predictions of the non-steady jet-formation theory and experiment may be due to either inaccuracies in the determination of the initial conditions for jet formation or inaccuracies in the treatment of the jet-formation process itself. The collapse velocities and jet velocities deduced by Eichelberger are shown in Figure 13.

The nature of the discrepancies between theory and experiment discovered by Eichelberger is illustrated in Figures 14 and 15. In Figure 14, the theoretical cumulative mass distribution in the jet (as a function of velocity) is compared to the results of several experimental mass determinations. In these tests, the jet first perforated a target plate then its tip was photographed with a high-speed camera, and finally the remaining jet was collected and the particles weighed. The jet tip velocity was determined from the photographs. The curve was computed from slug mass data using the "convergenceless" PER theory, assuming instantaneous acceleration of the liner elements by the detonating explosive and deflection of the liner segment according to the Taylor angle hypothesis.

*Reference 2, p. 536

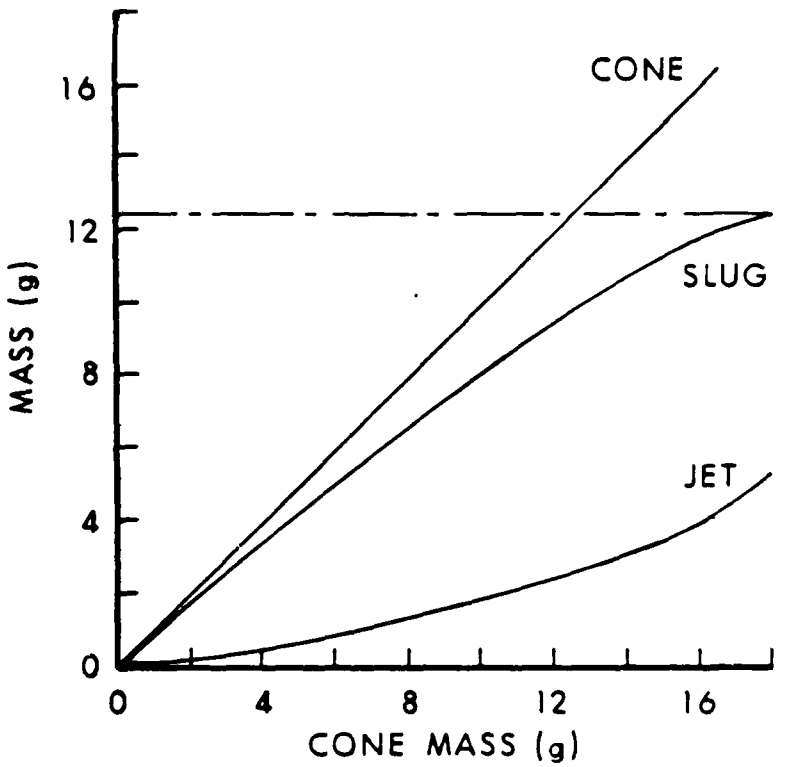

Figure 11. Eichelberger's results for mass of slug section as a function of mass of parent liner (from Reference 6).

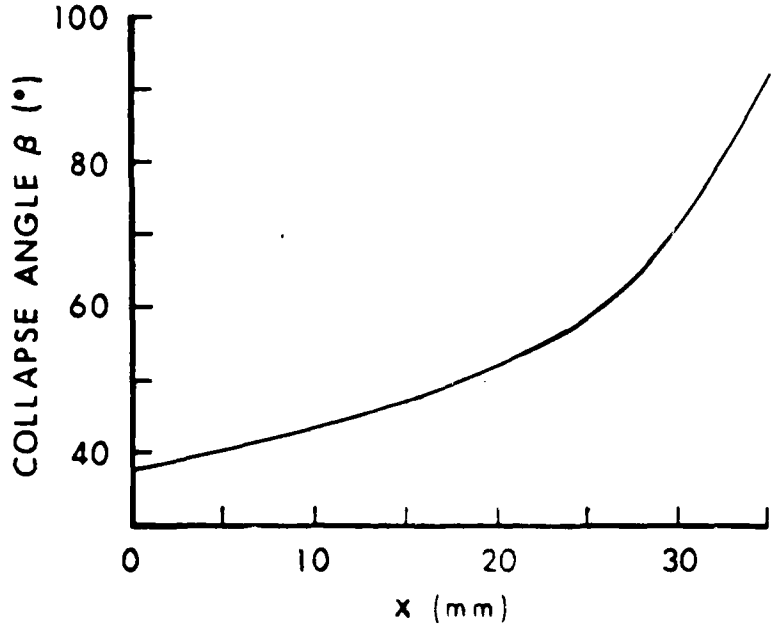

Figure 12. Eichelberger's plot of collapse angle β as a function of initial position of liner element, measured from top of cone (from Reference 6).

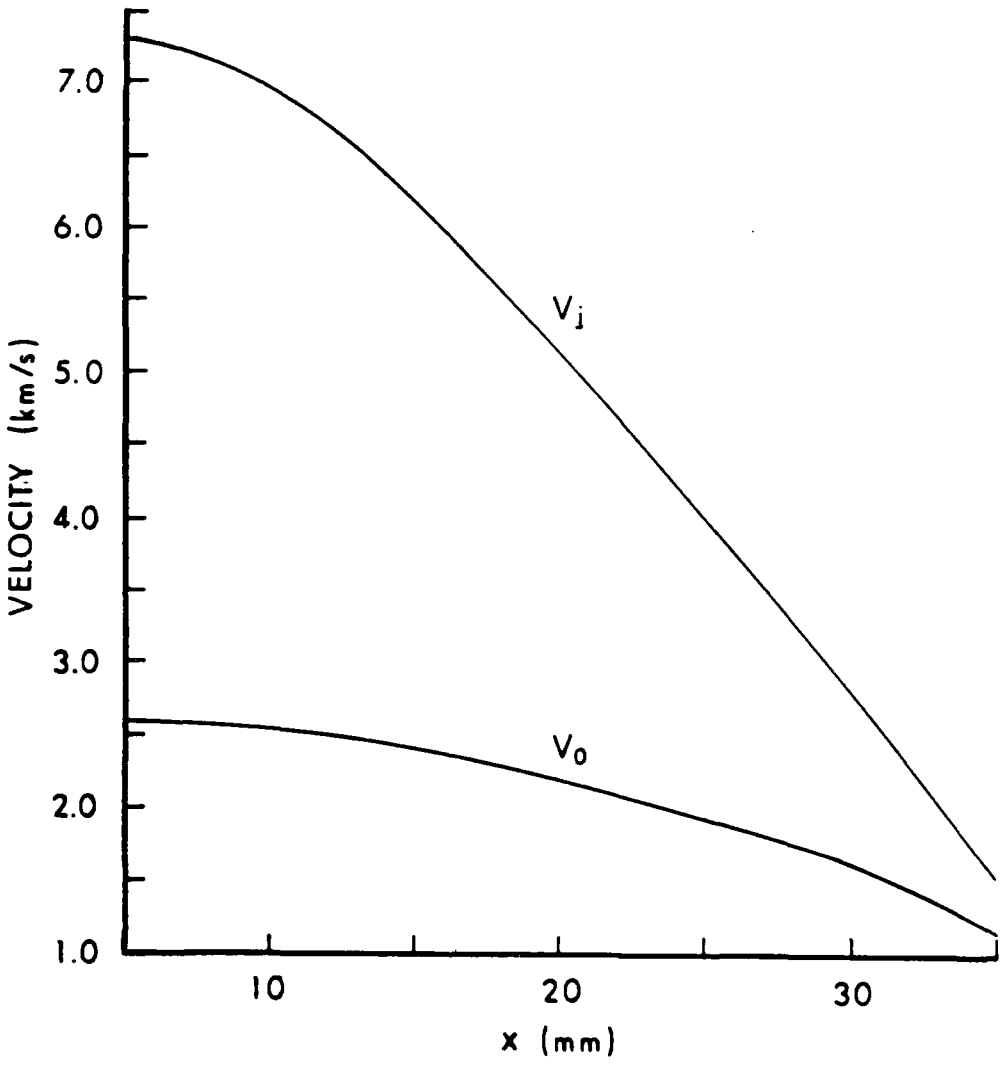

Figure 13. Eichelberger's computed values of collapse velocity V_o and t velocity V_j as functions of initial position of liner element (from Reference 6).

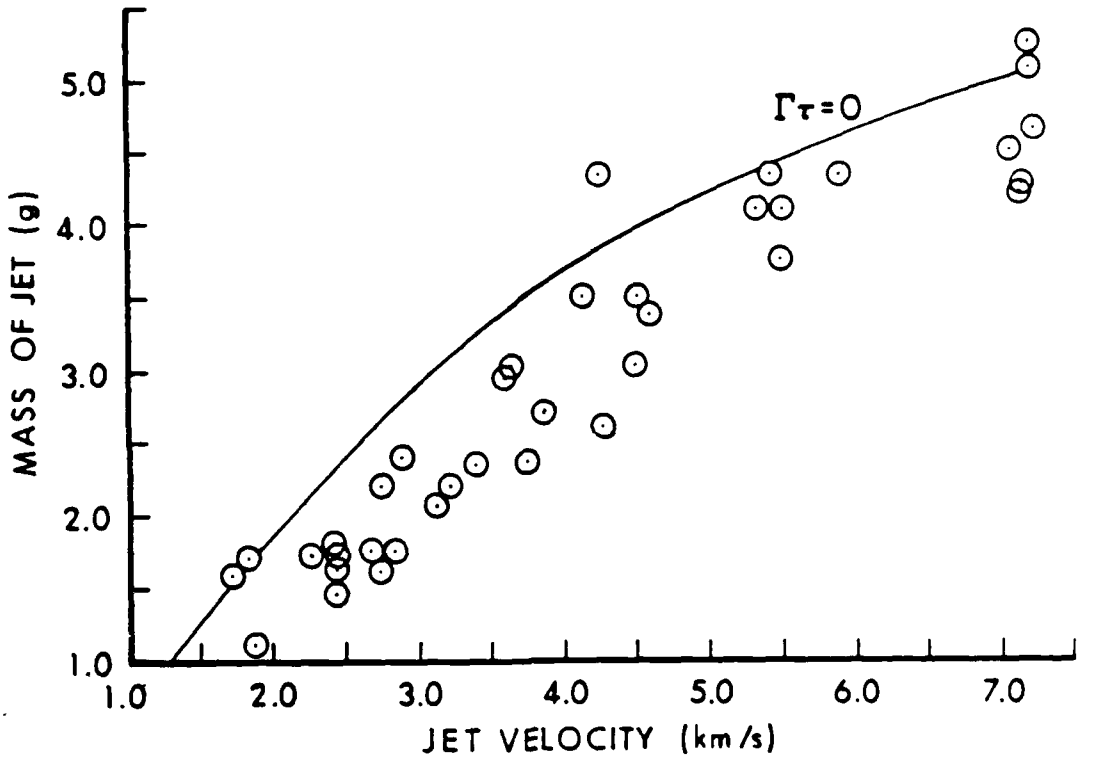

Figure 14. Comparison of computed distribution of mass in the jet with experimental observations as shown in Eichelberger's paper (from Reference 6).

In Figure 15, the theoretical spatial distribution of the jet velocities is displayed along with the experimental observations at a short time (35μs) after the detonation waves passed over the apex of the liner. The position of the jet tip relative to the detonation wave was used to fix the position of the tip for the theoretical curve. The experimental curve "leads" the theoretical curve, and the disagreement is greatest at the rear of the jet.

The jet-mass discrepancy may be due to the neglect of the convergence gradient in the treatment of the steady-state jet formation process. A qualitative explanation of the difference between the PER and the observed jet mass distribution may be obtained from the new theory. The differences between the jet properties calculated by the Birkhoff, MacDougall, Pugh and Taylor (BMPT) theory, using the collapse velocity and collapse angle of the central streamline of the liner, and the jet properties calculated by the new theory taking into account a linear convergence-velocity gradient of strength 0.1107 km s^{-1} mm^{-1} are illustrated in Table 7. For these "apparently identical" initial conditions, the new theory predicts a jet element with about 8 percent less mass and about 3 percent higher velocity than that of a jet element whose properties were estimated by the BMPT theory which ignores the convergence-velocity gradient. For the slug, the new theory predicts an element slightly more massive (less than 1 percent) and 13 percent faster than that estimated by the BMPT theory. If a correction of 92 percent in mass and 103 percent in velocity is applied to the curve of Figure 14, the new curve is in better agreement with the experimental data. This is shown in Figure 16. Of course, there is no reason to expect that the correction would be constant over the collapse of the entire liner, but it would require a calculation of the complete jet-formation process to find the actual corrections.

An explanation of the difference between the PER theoretical predictions and the observed jet position, probably requires more than just the new jet formation theory. In Figure 17, the point J on the axis of symmetry of the conical liner at which the jet is formed from a liner point originally at P is controlled by α, the half-angle of the cone apex and by the deflection angle δ. For steady-state collapse, the angle δ is the Taylor angle used in the PER theory for the case of the unsteady collapse. For liner collapse in which there is a velocity gradient along the length of the liner, as in the case of unsteady collapse, Chou, Hirsch and Ciccarelli [9], CHC, have shown that the deflection angle is no longer the Taylor angle, but depends on the collapse velocity gradient. Thus, both the collapse angle β and the deflection angle δ depend on the collapse velocity gradient along the length of the liner.

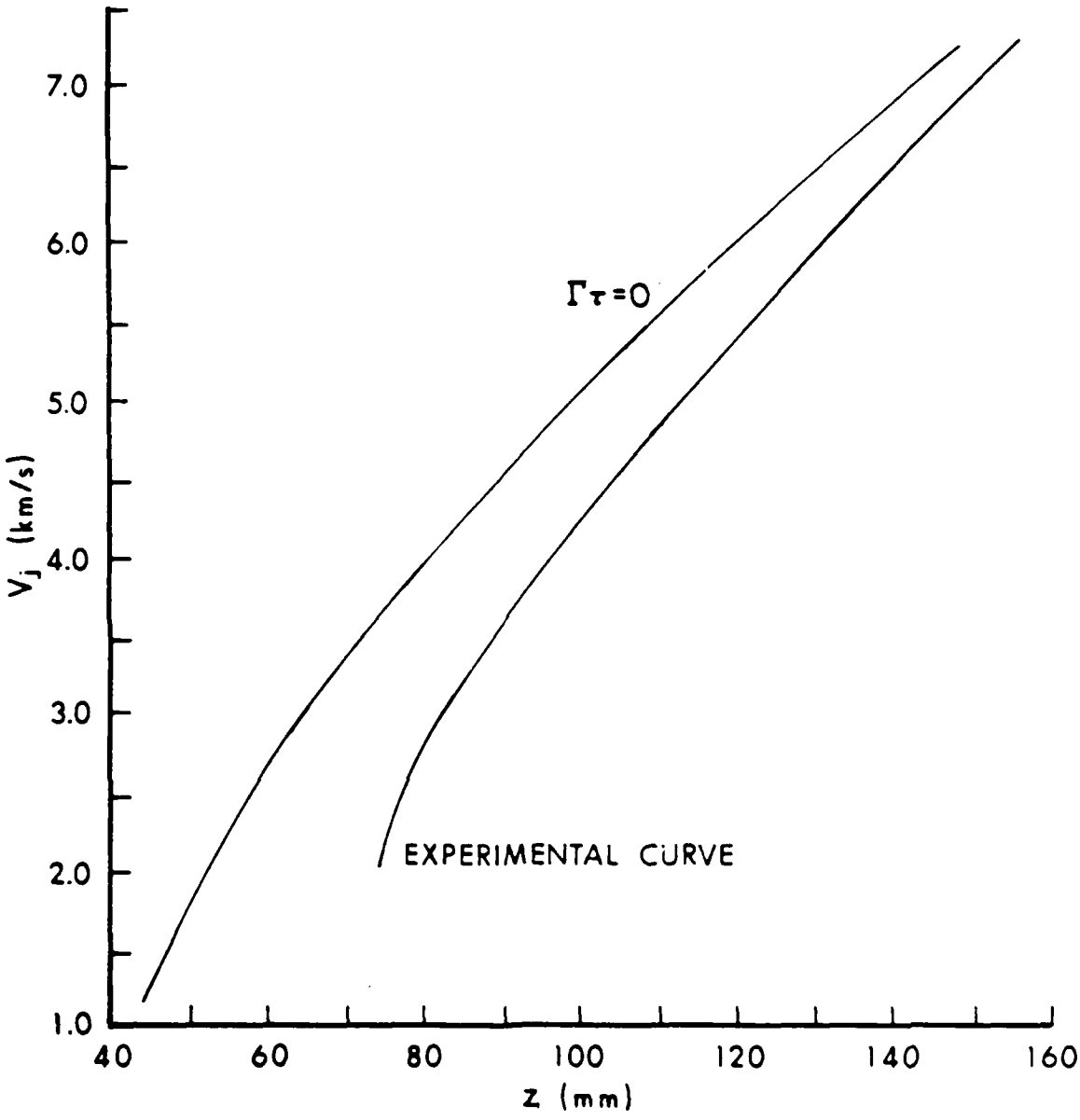

Figure 15. Comparison of comuted for $\Gamma_\tau = 0$) and observed distribution of velocities in the jet 35μs after initiation of the charge (from Reference 6).

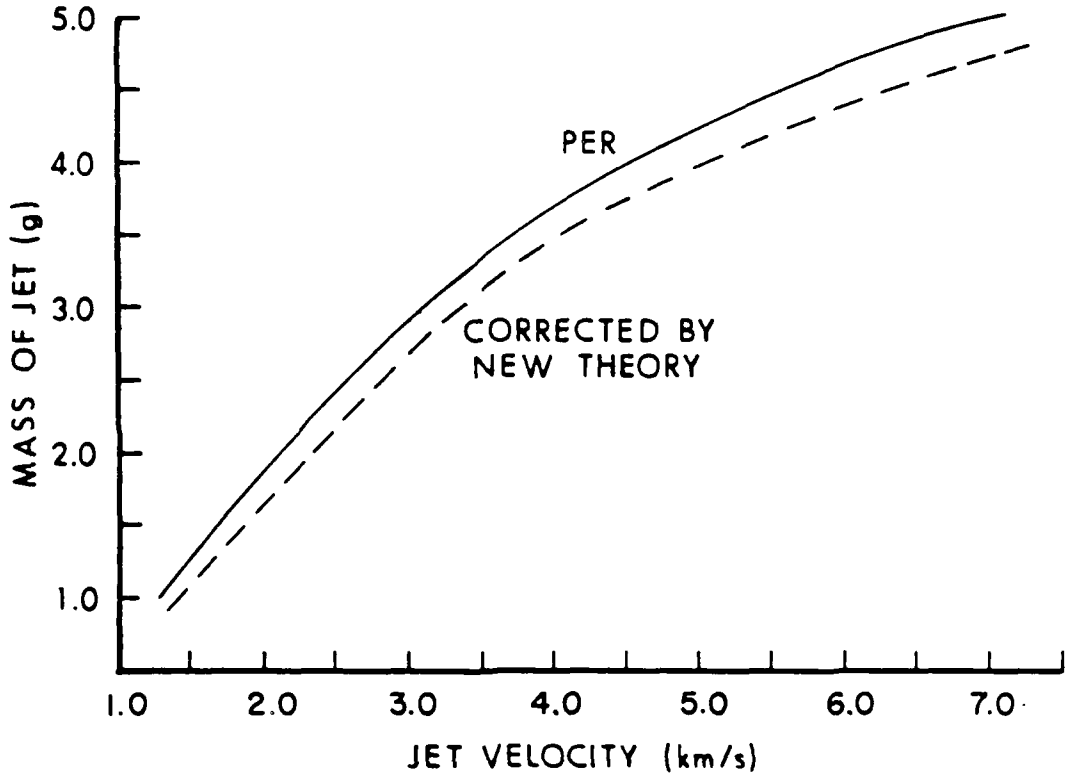

Figure 16. Nominal correction to PER theory applied on the basis of the results of the new theory.

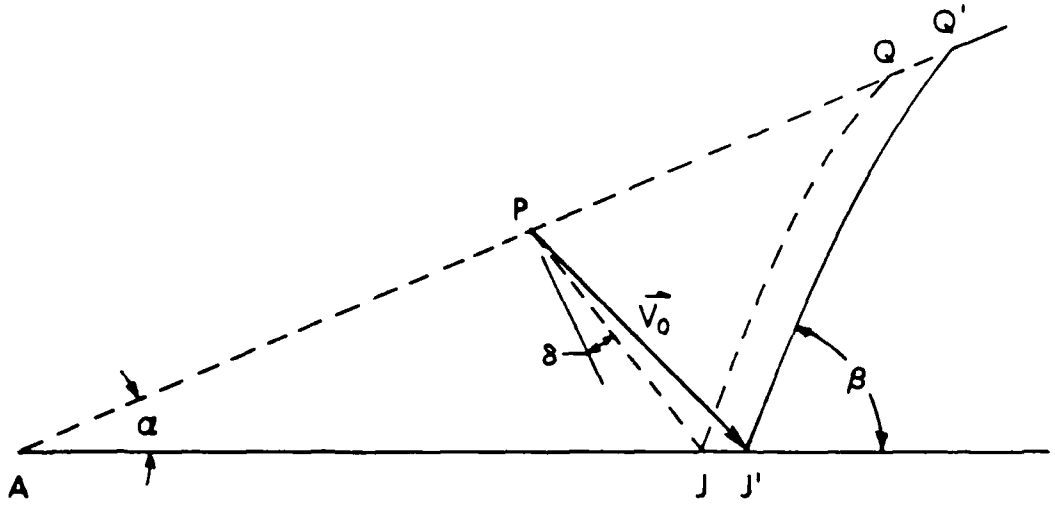

Figure 17. Illustrating the effect of an increase in the deflection angle on the jet formation position.

According to some calculations made by CHC for the collapse of the BRL 81mm shaped charge, the difference between the deflection angle "observed" in computer simulations of the cone collapse and the Taylor angle increases from some 13 percent near the apex to as much as 75-80 percent near the base of the cone.* Similar results would apply to the charge analyzed by Eichelberger, so it appears that the deflection angle was probably underestimated by PER and so the distance of the collapse point J from the cone apex was probably underestimated. The combination of revised input conditions and the slightly higher jet velocities obtained from the new theory may account for the position discrepancy at short times after formation.

Table 7. COMPARISON OF THEORETICAL RESULTS

QUANTITY IN STAGNATION-POINT FRAME	THEORY-EQUATION
1. Incoming Flow Velocity	
$\vec{V_F} = \vec{V_F}(9,15) = 3.038$ km/s	BMPT-(3.1)
$= \langle \vec{V_{FN}} \rangle = 2.997$ km/s	NEW-(6.8)
2. Incoming Flow Kinetic Energy	
$KE_{in} = 135.4$ kJ/cm	BMPT-(B.3)
$= 131.8$ kJ/cm	NEW-(C.3)
3. Outgoing Jet Flow Velocity	
$\vec{V_{F1}} = \vec{V_F} = 3.038$ km/s	BMPT-(3.3)
$= \lvert\langle \vec{V_{F1}} \rangle\rvert = 3.232$ km/s	NEW-(6.9)
4. Outgoing Jet Kinetic Energy	
$KE_{lout} = 13.2$ kJ/cm	BMPT
$= 14.2$ kJ/cm	NEW
5. Outgoing Slug Flow Velocity	
$\lvert\vec{V_{F2}}\rvert = \lvert\vec{V_F}\rvert = 3.038$ km/s	BMPT-(3.4)
$= \lvert\langle \vec{V_{F2}} \rangle\rvert = 2.969$ km/s	NEW-(6.10)

*Reference 9, p. 23.

6. Outgoing Slug Kinetic Energy

KE_{2out} = 122.2 kJ/cm BMPT

= 117.4 kJ/cm NEW

QUANTITY IN LAB FRAME FOR V_{SP} = 3.598 km/s THEORY-EQUATION

7. Jet Velocity

$\vec{V_j}$ = 6.636 km/s BMPT-(3.3)

= 6.830 km/s NEW

8. Jet Mass

$m_j = 0.0976\ m_1 = 2.865$ g/cm BMPT

$= 0.0899\ m_1 = 2.639$ g/cm NEW

9. Slug Velocity

$\vec{V_s}$ = 0.560 km/s BMPT-(3.4)

= 0.629 km/s NEW

10. Slug Mass

$m_s = 0.9024\ m_1 = 26.491$ g/cm BMPT

$= 0.9101\ m_1 = 26.717$ g/cm NEW

X. SUMMARY AND CONCLUSIONS

This study appears to be the first attempt to explicitly integrate convergence effects into the jet-formation equations. For initial conditions appropriate to a conventional conical-lined shaped charge, the predicted changes to the results of the previous theory are small, but in the proper direction to explain some of the discrepancies observed by Eichelberger.

The new theory, in both wedge and conical flow form, conserves mass, kinetic energy and linear momentum. Appendix A demonstrates the conservation of kinetic energy in wedge flow; Appendix B does the same for "uniform conical flow." Appendix C illustrates the key results in the demonstration of conservation of kinetic energy in nonuniform conical flow with a linear velocity gradient. For the rather artificial condition of constant energy influx and varying strength of the convergence-velocity gradient, the mass partitioning for the wedge flow is confined between $m_s/m_l = \cos^2(\beta/2)$ and $m_s/m_l = \cos(\beta/2)$, for positive values of the minimum collapse velocity V_{OF} in the case considered. Very similar results are found for the case of conical flow considered. It appears that the strengths of the convergence-velocity gradients for conventional conical liners lie in the range 0.1 to 0.2 km s^{-1} mm^{-1}.

A HEMP simulation of the collapse of the shaped charge used in Eichelberger's experiments and a calculation of the integrated effect of the convergence-velocity perturbation would be required to show whether the convergence-velocity effect alone is sufficient to bring theory and experiment into agreement. The HEMP code simulates the collapse dynamics of a shaped-charge liner rather accurately [10], but cannot properly form the jet and slug for most shaped-charge designs. The HEMP input would be used in the new jet formation equations since it "automatically" includes the unsteady collapse effects.

REFERENCES

1. Garrett Birkhoff, Duncan P. MacDougall, Emerson M. Pugh, and Sir Geoffrey Taylor, "Explosives with Lined Cavities," Journal of Applied Physics, Vol. 19, No. 6, pp. 563-582, June 1948.

2. Emerson M. Pugh, R.J. Eichelberger and Norman Rostoker, "Theory of Jet Formation by Charges with Lined Conical Cavities," Journal of Applied Phyics, Vol. 23, No. 5, pp. 532-536, May 1952.

3. R.J. Eichelberger and Emerson M. Pugh, "Experimental Verification of the Theory of Jet Formation by Charges with Lined Conical Cavities," Journal of Applied Physics, Vol. 23, No. 5, pp. 537-542, May 1952.

4. R.J. Eichelberger, "Re-Examination of the Nonsteady Theory of Jet Formation by Lined Cavity Charges," Journal of Applied Physics, Vol. 26, No.4, pp. 398-402, April 1955.

5. Theodore E. Sterne, "A Note on Collapsing Cylindrical Shells," Journal of Applied Physics, Vol. 21, No. 2, pp. 73-74, February 1950.

6. R.J. Eichelberger, Re-Examination of the Theories of Jet Formation and Target Penetration by Lined Cavity Charges, Carnegie Institute of Technology Contract Report CEL Report No. 1, June 1954.

7. Mark L. Wilkins, Calculation of Elastic-Plastic Flow, Lawrence Radiation Laboratory Report UCRL-7322, 1969.

8. Raymond T. Birge, "Least Squares' Fitting of Data by Means of Polynomials," Reviews of Modern Physics, Vol. 19, No. 4, pp. 298-360, 1947.

9. Pei Chi Chou, Eitan Hirsch and Robert D. Ciccarelli, An Unsteady Taylor Angle Formula for Liner Collapse, Ballistic Research Laboratory Contract Report ARBRL-CR-00461, August 1981.

10. Harrison, J. T. and Karpp, R. R., "Terminal Ballistic Application of Hydrodynamic Computer Code Calculations," Ballistic Research Laboratory Report No. 1984, April 1977.

APPENDIX A.

Conservation of Kinetic Energy in Wedge Flow

$$KE_{in} = \frac{1}{2} \rho a \int_o^a \frac{V^2(x)}{a} dx \tag{A-1}$$

$$= \frac{1}{2} \rho \int_o^a (V_o + \alpha x)^2 \, dx \tag{A-2}$$

$$= \rho \frac{V_o^2}{2} a + \rho \frac{\alpha V_o}{2} a^2 + \rho \frac{\alpha^2}{6} a^3 \tag{A-3}$$

$$KE_{out} = \frac{1}{2} \rho a_2 \int_o^{a_2} \frac{V^2(x')}{a_2} dx' + \frac{1}{2} \rho a_1 \int_o^{a_1} \frac{V^2(x'')}{a_1} dx'' \tag{A-4}$$

$$= \frac{1}{2} \rho \int_o^{a_2} (V_o + \alpha(a_2 - x'))^2 \, dx'$$

$$+ \frac{1}{2} \rho \int_o^{a_1} (V_o + \alpha(a_2 + x''))^2 \, dx''. \tag{A-5}$$

$$= \frac{1}{2} \rho V_o^2 (a_1 + a_2) + \rho \alpha V_o \left(\frac{a_2^2}{2} + a_2 a_1 + \frac{a_1^2}{2} \right)$$

$$+ \rho \alpha^2 \left(\frac{a_2^3}{6} + \frac{a_2^2 a_1}{2} + \frac{a_2 a_1^2}{2} + \frac{a_1^3}{6} \right) \tag{A-6}$$

$$= \rho \frac{V_o^2}{2} a + \rho \frac{\alpha V_o}{2} a^2 + \rho \frac{\alpha^2 a^3}{6} \tag{A-7}$$

where $a_1 + a_2 = a$

APPENDIX B

Conservation of Kinetic Energy in
"Uniform Conical Flow"

$$KE_{in} = \frac{1}{2} \rho A_o \int_o^a \frac{V_o^2}{A_o} 2\pi(r_C - \varepsilon x)dx \tag{B-1}$$

$$= \pi\rho V_o^2 \int_o^a (r_C - \varepsilon x)dx \tag{B-2}$$

$$= \pi\rho V_o^2 a \left[r_C - \varepsilon a/2\right] \tag{B-3}$$

$$KE_{out} = \frac{1}{2} \rho A_1 \int_o^{a_1} \frac{V_o^2}{A_1} 2\pi x''dx''$$

$$+ \frac{1}{2} \rho A_2 \int_o^{a_2} \frac{V_o^2}{A_2} 2\pi x'dx' \tag{B-4}$$

$$= \pi\rho \frac{V_o^2}{2} (a_1^2 + a_2^2) = \pi\rho \frac{V_o^2}{2} (r_C + r_E)a \tag{B-5}$$

$$= \pi\rho V_o^2 a\left[r_C - \varepsilon a/2\right] \tag{B-6}$$

APPENDIX C

Conservation of Kinetic Energy in Nonuniform Conical Flow With Linear Velocity Gradient

$$KE_{in} = \frac{1}{2} \rho A_o \int_o^a \frac{V_{FN}^2(x)}{A_o} 2\pi (r_C - \varepsilon x) dx \tag{C-1}$$

$$= \pi \rho \int_o^a (V_{OFN} + \alpha x)^2 (r_C - \varepsilon x) dx \tag{C-2}$$

$$= \pi \rho \left[r_C V_{OFN}^2 a + (2\alpha r_C - \varepsilon V_{OFN}) V_{OFN} \frac{a^2}{2} \right.$$

$$\left. + (r_C \alpha^2 - 2\varepsilon\alpha V_{OFN}) \frac{a^3}{3} - \varepsilon\alpha^2 a^4/4 \right] \tag{C-3}$$

The fraction of the area of the incoming flow through which the jet material passes is illustrated in Figure C-1. The area intercepted by the incoming jet flow is

$$A_{y'} = \pi y' (r_{a_2^*} + r_{y'}) \quad , \tag{C-4}$$

where $$r_{y'} = r_{a_2^*} - \varepsilon y' \quad , \tag{C-5}$$

and $$r_{a_2^*} = r_C - \varepsilon a_2^* \quad . \tag{C-6}$$

Then $$A_{y'} = \pi y' (2r_C - 2\varepsilon a_2^* - \varepsilon y') \tag{C-7}$$

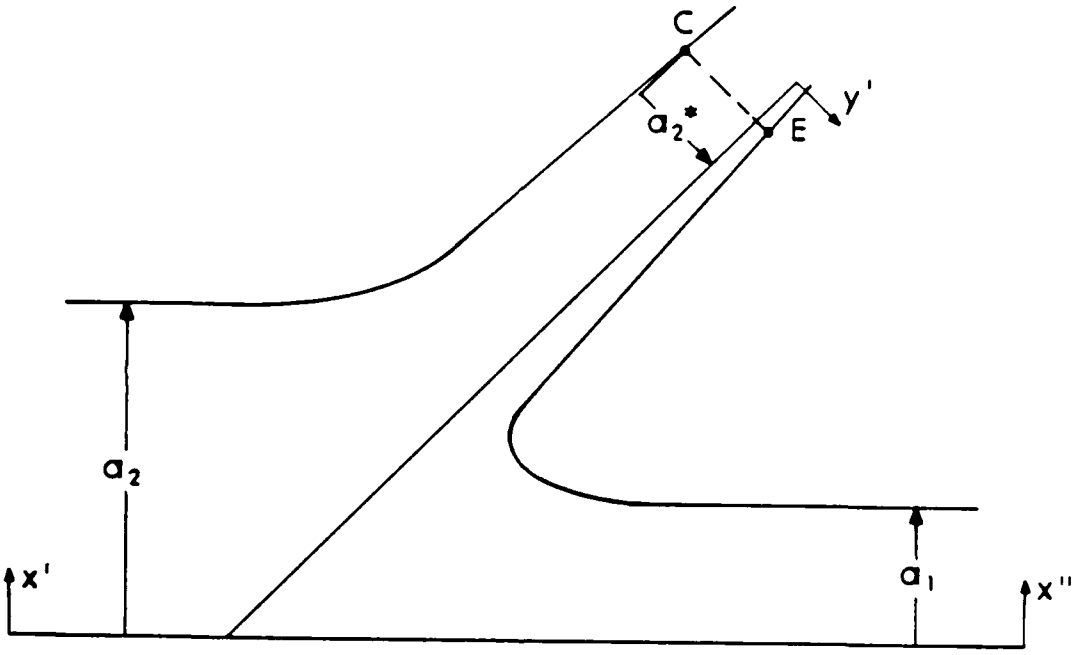

Figure C-1. Determination of flow areas.

These same streamlines, further from a^*, intersect the area $A_{x''}$ in the outgoing jet flow, where

$$A_{x''} = \pi x''^2 \quad . \tag{C-8}$$

Since the flow is incompressible,

$$A_{x''} = A_{y'} \tag{C-9}$$

and
$$y'(2r_c - 2\varepsilon a_2^* - \varepsilon y') = x''^2 \quad . \tag{C-10}$$

Then
$$y' = \frac{A}{\varepsilon}(a_2^*) - \frac{\sqrt{A^2(a_2^*) - \varepsilon x''^2}}{\varepsilon} \tag{C-11}$$

where
$$A(a_2^*) \equiv r_c - \varepsilon a_2^* \tag{C-12}$$

gives the streamline spacing relation. Note that, when $y' = 0$, $x'' = 0$, and when $y' = a - a_2^*$, $x'' = \dfrac{[(r_c - \varepsilon a_2^*)^2 - (r_c - \varepsilon a)^2]^{1/2}}{\varepsilon} = a_1$.

$$KE_{out} = \frac{1}{2}\rho A_1 \int_0^{a_1} \frac{[V''_{FN}(x'')]^2}{A_1} 2\pi x''dx''$$

$$+ \frac{1}{2}\rho A_2 \int_0^{a_2} \frac{[V'_{FN}(x')]^2}{A_2} 2\pi x'dx' \tag{C-13}$$

where the first term represents the energy per unit length in the jet and the second the energy per unit length in the slug.

For the slug,

$$V'_{FN}(x') = V_{OFN} + \alpha a_2^* + \frac{\alpha}{\varepsilon} A(a_2^*) - \frac{\alpha}{\varepsilon}\sqrt{A^2(a_2^*) + \varepsilon x'^2} \quad , \tag{C-14}$$

where $$a_2^* = \frac{r_C - (r_C^2 - \varepsilon a_2^2)^{1/2}}{\varepsilon} \quad , \tag{C-15}$$

and $$A(a_2^*) = r_C - \varepsilon a_2^* = (r_C^2 - \varepsilon a_2^2)^{1/2} \quad . \tag{C-16}$$

For the jet,

$$V''_{FN}(x'') = V_{FN}(a_2^*) + \alpha y' \tag{C-17}$$

$$= V_{OFN} + \alpha a_2^* + \frac{\alpha}{\varepsilon} A(a_2^*) - \frac{\alpha}{\varepsilon}\sqrt{A^2(a_2^*) - \varepsilon x''^2} \tag{C-18}$$

Note that $V'_{FN}(x')$ decreases as x' increases, while $V''_{FN}(x'')$ increases as x" increases.

Substituting Eqs. (C-14) and (C-18) into Eq. (C-13) and integrating gives

$$KE_{out} = \pi\rho \left\{ V_{OFN}^2 \frac{a_2^2}{2} + \alpha V_{OFN} a_2^* a_2^2 + \frac{1}{2}\alpha^2 a_2^2 (a_2^*)^2 \right.$$

$$\left. - \frac{2\alpha}{3\varepsilon^2} V_{OFN}\left[A^2(a_2^*) + \varepsilon a_2^2\right]^{3/2} + \frac{\alpha}{\varepsilon} V_{OFN} A(a_2^*) a_2^2 \right.$$

$$+ \frac{\alpha^2}{\varepsilon} a_2^* A(a_2^*) a_2^2 + \frac{\alpha^2}{\varepsilon^2} A^2(a_2^*) \frac{a_2^2}{2}$$

$$- \frac{2}{3} \frac{\alpha^2}{\varepsilon^2} a_2^* \left[A^2(a_2^*) + \varepsilon a_2^2 \right]^{3/2}$$

$$- \frac{2}{3} \frac{\alpha^2}{\varepsilon^2} A(a_2^*) \left[A^2(a_2^*) + \varepsilon a_2^2 \right]^{3/2} + \frac{\alpha^2}{\varepsilon^2} A^2(a_2^*) \frac{a_2^2}{2} + \frac{\alpha^2}{4\varepsilon} a_2^4 \Bigg\}$$

$$+ \Bigg\{ V_{OFN}^2 \frac{a_1^2}{2} + \alpha V_{OFN} a_2^* a_1^2 + \alpha^2 a_2^{*2} \frac{a_1^2}{2}$$

$$+ \frac{2\alpha}{3\varepsilon^2} V_{OFN} \left[A^2(a_2^*) - \varepsilon a_1^2 \right]^{3/2}$$

$$+ \frac{\alpha}{\varepsilon} V_{OFN} A(a_2^*) a_1^2 + \frac{\alpha^2}{\varepsilon} a_2^* A(a_2^*) a_1^2$$

$$+ \frac{\alpha^2}{\varepsilon^2} A^2(a_2^*) \frac{a_1^2}{2} + \frac{2}{3} \frac{\alpha^2}{\varepsilon^2} a_2^* \left[A^2(a_2^*) - \varepsilon a_1^2 \right]^{3/2}$$

$$+ \frac{2}{3} \frac{\alpha^2}{\varepsilon^2} A(a_2^*) \left[A^2(a_2^*) - \varepsilon a_1^2 \right]^{3/2}$$

$$+ \frac{\alpha^2}{\varepsilon^2} A^2(a_2^*) \frac{a_1^2}{2} - \frac{\alpha^2}{4\varepsilon} a_1^4 \Bigg\} \qquad \text{(C-19)}$$

Now $$a_1^2 = (r_C + r_E)a - a_2^2 \qquad \text{(C-20)}$$

$$= 2r_C a - \varepsilon a^2 - a_2^2 \ . \qquad \text{(C-21)}$$

Then $KE_{out} = \pi \left\{ -\frac{2}{3} \frac{\alpha}{\varepsilon^2} V_{OFN} r_C^2 - \frac{2}{3} \frac{\alpha^2}{\varepsilon^2} a_2^* r^2 \right.$

$$- \frac{2}{3} \frac{\alpha^2}{\varepsilon^2} (r_C^2 - \varepsilon a_2^2)^{1/2} r_C^2 + \frac{\alpha^2}{4\varepsilon} a_2^4 \Bigg\}$$

$$+ \pi \Bigg\{ \Bigg[r_C V_{OFN}^2 + 2\alpha r_C a_2^* V_{OFN} + \alpha^2 a_2^{*2} r_C$$

$$+ 2\frac{\alpha}{\varepsilon} V_{OFN} r_C (r_C^2 - \varepsilon a_2^2)^{1/2}$$

$$+ 2 \frac{\alpha^2}{\varepsilon} r_C a_2^* (r_C^2 - \varepsilon a_2^2)^{1/2}$$

$$+ 2 \frac{\alpha^2}{\varepsilon^2} r_C (r_C^2 - \varepsilon a_2^2)^{1/2} \Bigg] a$$

$$+ \Bigg[-\varepsilon \frac{V_{OFN}^2}{2} - \alpha\varepsilon V_{OFN} a_2^* - \alpha^2 \varepsilon \frac{a_2^{*2}}{2}$$

$$- \alpha V_{OFN} (r_C^2 - \varepsilon a_2^2)^{1/2} - \alpha^2 a_2^* (r_C^2 - \varepsilon a_2^2)^{1/2}$$

$$- \frac{\alpha^2}{\varepsilon} r_C^2 + \alpha^2 a_2^2 \Bigg] a^2$$

$$+ \frac{2}{3} \frac{\alpha}{\varepsilon^2} V_{OFN} \left[r_C^2 - 2\varepsilon r_C a + \varepsilon^2 a^2 \right]^{3/2}$$

$$+ \frac{2}{3} \frac{\alpha^2}{\varepsilon^2} a_2^* \left[r_C^2 - 2\varepsilon r_C a + \varepsilon^2 a^2 \right]^{3/2}$$

$$+ \frac{2}{3} \frac{\alpha^2}{\varepsilon^2} (r_C^2 - \varepsilon a_2^2)^{1/2} \left[r_C^2 - 2 r_C \varepsilon a + \varepsilon^2 a^2 \right]^{3/2}$$

$$- \frac{\alpha^2}{4\varepsilon} a_1^4 \Bigg\} \qquad (C\text{-}22)$$

Now, $a_2^* = \dfrac{r_c - (r_c^2 - \varepsilon a^2)^{1/2}}{\varepsilon}$, so, after simplification,

$$KE_{out} = \pi \left\{ r_c a\, V_{OFN}^2 + \left[2\alpha r_c - \varepsilon V_{OFN} \right] V_{OFN}\, a^2/2 \right.$$

$$\left. + \left(\alpha^2 r_c - 2\alpha\varepsilon V_{OFN}\right) a^3/3 - \varepsilon \frac{\alpha^2}{4} a^4 \right\} \qquad \text{(C-23)}$$

DISTRIBUTION LIST

No. of Copies	Organization
12	Administrator Defense Technical Info Center ATTN: DTIC-DDA Cameron Station Alexandria, VA 22304-6145
1	HQDA (DAMA-ART-M) Washington, DC 20310
1	Commander US Army Materiel Command ATTN: AMCDRA-ST 5001 Eisenhower Avenue Alexandria, VA 22333-0001
1	Commander Armament R&D Center US Army AMCCOM ATTN: SMCAR-TSS Dover, NJ 07801
1	Commander Armament R&D Center US Army AMCCOM ATTN: SMCAR-TDC Dover, NJ 07801
1	Director Benet Weapons Laboratory Armament R&D Center US Army AMCCOM ATTN: SMCAR-LCB-TL Watervliet, NY 12189
1	Commander US Army Armament, Munitions and Chemical Command ATTN: SMCAR-ESP-L Rock Island, IL 61299
1	Commander US Army Aviation Research and Development Command ATTN: AMSAV-E 4300 Goodfellow Blvd St. Louis, MO 63120
1	Director US Army Air Mobility Research and Development Laboratory Ames Research Center Moffett Field, CA 94035
1	Commander US Army Communications-Electronics Command ATTN: AMSEL-ED Fort Monmouth, NJ 07703
1	Commander ERADCOM Technical Library ATTN: DELSD-L (Reports Section) Fort Monmouth, NJ 07703-5301
1	Commander US Army Missile Command Research, Development and Engineering Center ATTN: AMSMI-RD Redstone Arsenal, AL 35898
1	Director US Army Missile & Space Intelligence Center ATTN: AIAMS-YDL Redstone Arsenal AL 35898-5500
1	Commander US Army Tank-Automotive Cmd ATTN: AMSTA-TSL Warren, MI 48397-5000
1	Director US Army TRADOC Systems Analysis Activity ATTN: ATAA-SL White Sands Missile Range NM 88002
1	Commandant US Army Infantry School ATTN: ATSH-CD-CSO-OR Fort Benning, GA 31905

DISTRIBUTION LIST

No. of Copies	Organization
1	Commander US Army Development and Employment Agency ATTN: MODE-TED-SAB Fort Lewis, WA 98433
1	AFWL/SUL Kirtland AFB, NM 87117
1	AFATL/DLODL Eglin AFB, FL 32542-5000
10	Central Intelligence Agency Office of Central Reference Dissemination Branch Room GE-47 HQS Washington, DC 20502
1	AAI ATTN: A. Farinocci P. O. Box 6767 Baltimore, MD 21204
1	Northrop Corporation Electro-Mechanical Division ATTN: Donald L. Hall 500 East Orangethorpe Avenue Anaheim, CA 92801
1	Boeing Aerospace Co. Shock Physics & Applied Math Engineering Technology ATTN: R. Helzer P. O. Box 3999 Seattle, WA 98124
1	McDonnell Douglas Astronautics Company ATTN: Bruce L. Cooper 5301 Bolsa Avenue Huntington Beach, CA 92647
1	D. R. Kennedy and Associates, Inc. ATTN: Donald Kennedy P. O. Box 4003 Mountain View, CA 94040
2	Dyna East Corporation ATTN: P. C. Chou R. Ciccarelli 3432 Market Street Philadelphia, PA 19104-2588
1	Physics International Company Tactical Systems Group Eastern Division ATTN: R. Berus P. O. Box 1004 Wadsworth, OH 44281-0904
2	Sandia Laboratories ATTN: Alan Robinson, Marlin Kipp Albuquerque, NM 87115
1	Aerojet Ordnance Corporation ATTN: Warhead Tech. Dept. Dr. J. Carleone 2521 Michelle Drive Tustin, CA 92680
1	Systems, Science & Software ATTN: Dr. R. Sedgwick P. O. Box 1620 La Jolla, CA 92037
1	AFATL/DL JR (J. Foster) Eglin, AFB, FL 32542
3	University of California Los Alamos Scientific Lab ATTN: Dr. J. Walsh Dr. R. Karpp Technical Library P. O. Box 1663 Los Alamos, NM 87545
2	California Research and Technology ATTN: Dr. Ronald E. Brown Dr. Mike Murphy 11875 Dublin Blvd. Suite B-130 Dublin, CA 94568

DISTRIBUTION LIST

No. of Copies	Organization
1	Zernow Technical Services, Inc. 425 West Bonita Avenue Suite 208 San Dimas, CA 91773
2	Director Lawrence Livermore Laboratory ATTN: Dr. M. Van Thiel Technical Library P. O. Box 808 Livermore, CA 94550
1	Honeywell, Inc. Defense Systems Division ATTN: Joel Houlton 5901 S. County Rd. 18 Edina, MN 55436
1	Goodyear Aerospace Corporation Tactical Weapon Systems Engineering Defense Systems Division ATTN: Roy L. Woodall 1210 Massillon Road Akron, OH 44315

No. of Copies	Organization
	Aberdeen Proving Ground
	Dir, USAMSAA ATTN: AMXSY-D AMXSY-MP (H. Cohen) AMXSY-GI (B. Simmons)
	Cdr, USATECOM ATTN: AMSTE-TO-F
	Cdr, CRDC, AMCCOM ATTN: SMCCR-RSP-A SMCCR-MU SMCCR-SPS-IL

USER EVALUATION SHEET/CHANGE OF ADDRESS

This Laboratory undertakes a continuing effort to improve the quality of the reports it publishes. Your comments/answers to the items/questions below will aid us in our efforts.

1. BRL Report Number_____ Date of Report_____

2. Date Report Received_____

3. Does this report satisfy a need? (Comment on purpose, related project, or other area of interest for which the report will be used.)_____

4. How specifically, is the report being used? (Information source, design data, procedure, source of ideas, etc.)_____

5. Has the information in this report led to any quantitative savings as far as man-hours or dollars saved, operating costs avoided or efficiencies achieved, etc? If so, please elaborate._____

6. General Comments. What do you think should be changed to improve future reports? (Indicate changes to organization, technical content, format, etc.)

CURRENT ADDRESS

Name

Organization

Address

City, State, Zip

7. If indicating a Change of Address or Address Correction, please provide the New or Correct Address in Block 6 above and the Old or Incorrect address below.

OLD ADDRESS

Name

Organization

Address

City, State, Zip

(Remove this sheet, fold as indicated, staple or tape closed, and mail.)

FOLD HERE

Director
US Army Ballistic Research Laboratory
ATTN: DRXBR-OD-ST
Aberdeen Proving Ground, MD 21005-5066

NO POSTAGE
NECESSARY
IF MAILED
IN THE
UNITED STATES

OFFICIAL BUSINESS
PENALTY FOR PRIVATE USE, $300

BUSINESS REPLY MAIL
FIRST CLASS PERMIT NO 12062 WASHINGTON, DC
POSTAGE WILL BE PAID BY DEPARTMENT OF THE ARMY

Director
US Army Ballistic Research Laboratory
ATTN: DRXBR-OD-ST
Aberdeen Proving Ground, MD 21005-9989

FOLD HERE